APPENDIX A - PART 1
FLUID FLOW AT SMALL ROTATING CYLINDER ELECTRODE

Mathcad 12 (2005) was used to undertake all the calculations shown in this Appendix. This program firstly calculates the kinematic viscosity and diffusion coefficient of cupric ions at different temperatures from the raw data collected from the literature (Ref. 1-4). It then derives the Reynolds and Taylor numbers to charaterize the fluid flow at the small and large RCE. Finally it uses these numbers to calculate the limiting current density and diffusion layer thickness, δ. The calculated limiting current density and δ are then compared with the experimental data.

The following table provides the raw data from the literature. An exponential curve was fitted to the raw data to obtain the absolute viscosity and diffusion of cupric ions data at the temperatures of interest.

TABLE 1

Temperature C	Fitted-Data Absolute Viscosity μ	Original Density Data(1)*, ρ	Fitted-Data Diffusion Coefficient Cupric Ions, D		Original Data (1)* Absolute Viscosity μodata	Original Data (2-4)* Diffusion Coefficient Cupric Ions DO
	$\frac{g}{cm\cdot s}$*	$\frac{g}{cm^3}$*	$\frac{cm^2}{s}$*	RPM*	$\frac{g}{cm\cdot s}$*	$\frac{cm^2}{s}$*

data :=

	0	1	2	3	4	5	6
0	20	0.019	1.186	$6\cdot10^{-6}$	10	0.019	$5\cdot10^{-6}$
1	25	0.017	1.183	$7\cdot10^{-6}$	10	0	$4.81\cdot10^{-6}$
2	30	0.015	1.18	$8\cdot10^{-6}$	15	0.015	$7.8\cdot10^{-6}$
3	40	0.012	1.174	$1\cdot10^{-5}$	20	0.012	$9.5\cdot10^{-6}$
4	45	0.011	1.173	$1.1\cdot10^{-5}$	25	0	$9.16\cdot10^{-6}$
5	50	$9.8\cdot10^{-3}$	1.168	$1.2\cdot10^{-5}$	30	$9.79\cdot10^{-3}$	0
6	55	$9.05\cdot10^{-3}$	1.165	$1.3\cdot10^{-5}$	35	0	$1\cdot10^{-5}$
7	60	$8.3\cdot10^{-3}$	1.161	$1.4\cdot10^{-5}$	40	$8.27\cdot10^{-3}$	0
8	65	$7.5\cdot10^{-3}$	1.15	$1.5\cdot10^{-5}$	45	0	$1.62\cdot10^{-5}$

$i := 0..8$*

$T := data^{\langle 0 \rangle}$*

$\mu := \left(data \cdot \frac{g}{cm\cdot s}\right)^{\langle 1 \rangle}$*

$\rho := \left(data \cdot \frac{g}{cm^3}\right)^{\langle 2 \rangle}$*

$D := \left(data \cdot \frac{cm^2}{s}\right)^{\langle 3 \rangle}$*

$RPM := data^{\langle 4 \rangle}$*

$\mu odata := \left(data \cdot \frac{g}{cm\cdot s}\right)^{\langle 5 \rangle}$*

$DO := \left(data \cdot \frac{cm^2}{s}\right)^{\langle 6 \rangle}$*

* References in brackets. The ZERO value in the Table 1 means NOT AVAILABLE data.

CALCULATION OF KINEMATIC VISCOSITY, μ/ρ (cm^2/s)

ν = kinematic viscosity - fitted data

ν = kinematic viscosity - original data

$$\nu_i := \frac{\mu_i}{\rho_i} *$$

$$N_i := \frac{\mu odata_i}{\rho_i} *$$

$\nu_i =$ *

$1.573 \cdot 10^{-6}$	$m^2 \cdot s^{-1}$
$1.41 \cdot 10^{-6}$	
$1.246 \cdot 10^{-6}$	
$1.005 \cdot 10^{-6}$	
$9.207 \cdot 10^{-7}$	
$8.39 \cdot 10^{-7}$	
$7.772 \cdot 10^{-7}$	
$7.149 \cdot 10^{-7}$	
$6.522 \cdot 10^{-7}$	

$T_i =$

20
25
30
40
45
50
55
60
65

$N_i =$ *

0.01573	stokes
0	
0.01242	
0.01005	
0	
$8.38185 \cdot 10^{-3}$	
0	
$7.12317 \cdot 10^{-3}$	
0	

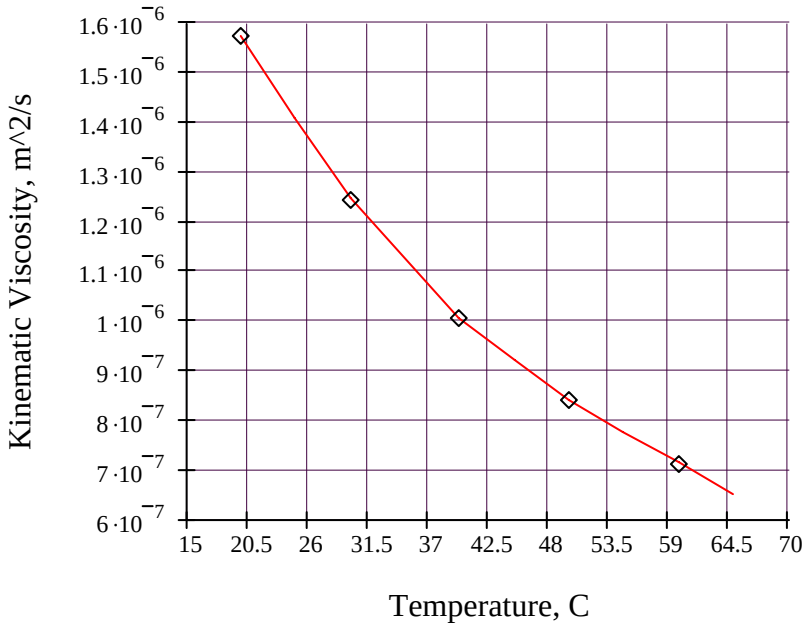

Figure 1. Plot of the Effect of Temperature on Kinematic Viscosity
Original Data (point) and Fitted Data (line)

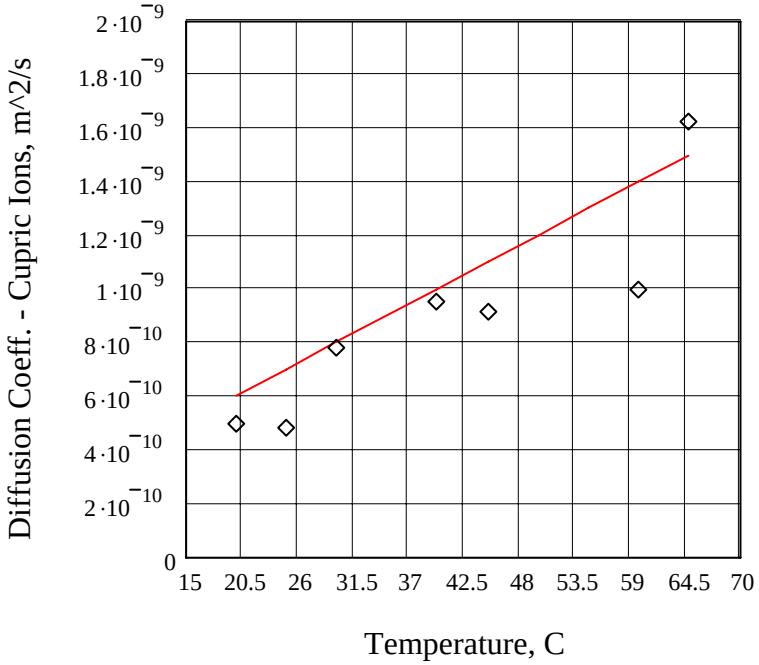

Figure 2. Plot on the Effect of Temperature on the Diffusion Coefficient of Cupric Ions
Original Data (point) and Fitted Data (line)

CALCULATION OF DIFFUSION LAYER THICKNESS USING THE NERNST EQUATION FOR THE SMALL RCE

$$Co := \frac{36\cdot 10^{-3}\ \frac{mol}{cm^3}}{63.546}$$ *

$n := 2$ *

$$F \equiv \frac{96485.3A\cdot s}{mol}$$ *

$di := 1.2cm$ * di is the diameter of the inner RCE, the rotating electrode.

$do := 7.6cm$ * do is the diameter of the outer RCE, stationary electrode.

$ri := \frac{di}{2}$ * $ro := \frac{do}{2}$ * $d := ro - ri$ d is the annulus, interelectrode distance

1. CALCULATION OF SCHMIDT NUMBERS, Sc

Sc numbers at their corresponding temperatures

$$Sc_i := \frac{\nu_i}{D_i}$$ *

$$Sc = \begin{pmatrix} 2622 \\ 2014 \\ 1557 \\ 1005 \\ 837 \\ 699 \\ 598 \\ 511 \\ 435 \end{pmatrix}$$ * $$T = \begin{pmatrix} 20 \\ 25 \\ 30 \\ 40 \\ 45 \\ 50 \\ 55 \\ 60 \\ 65 \end{pmatrix}$$

The Schmidt number varies from 435 at 65 degree C to 2736 at 20 degreeC.

2. CALCULATION OF REYNOLDS NUMBERS, Re

2.1 Calculation of Angular Velocity and Peripheral Velocity

Angular Velocity, ω

$$\omega_i := 2\pi \cdot \frac{RPM_i}{60 \cdot s}*$$

$$\omega = \begin{pmatrix} 1.047 \\ 1.047 \\ 1.571 \\ 2.094 \\ 2.618 \\ 3.142 \\ 3.665 \\ 4.189 \\ 4.712 \end{pmatrix} \frac{1}{sec}*$$

Peripheral Velocity, U

$$U_i := RPM_i \cdot \pi \cdot \frac{di}{60s}*$$

$$U = \begin{pmatrix} 0.628 \\ 0.628 \\ 0.942 \\ 1.257 \\ 1.571 \\ 1.885 \\ 2.199 \\ 2.513 \\ 2.827 \end{pmatrix} \frac{cm}{s}*$$

2.2 Calculation of Reynolds number according to J. Newman, Electrochemical Systems, **2004**, pp. 399: Re=d^2*ω/2ν ; DR Gabe and FC Walsh, J. App. Electrochemistry, 14, **1984**, pp. 555-564: Re=U*d/ν and Eisenberg, M, Tobias, and Wilke, C., J. Electrochem. Soc., **1954**, 101, 6, 306-319.

$$ReNewman_i := \frac{\omega_i \, di^2}{2 \nu_i}*$$

$$ReNewman = \begin{pmatrix} 48 \\ 53 \\ 91 \\ 150 \\ 205 \\ 270 \\ 340 \\ 422 \\ 520 \end{pmatrix}* \qquad RPM = \begin{pmatrix} 10 \\ 10 \\ 15 \\ 20 \\ 25 \\ 30 \\ 35 \\ 40 \\ 45 \end{pmatrix} \qquad T = \begin{pmatrix} 20 \\ 25 \\ 30 \\ 40 \\ 45 \\ 50 \\ 55 \\ 60 \\ 65 \end{pmatrix}$$

$$ReGabe_i := U_i \cdot \frac{di}{\nu_i}*$$

$$ReGabe = \begin{pmatrix} 48 \\ 53 \\ 91 \\ 150 \\ 205 \\ 270 \\ 340 \\ 422 \\ 520 \end{pmatrix}* \qquad RPM = \begin{pmatrix} 10 \\ 10 \\ 15 \\ 20 \\ 25 \\ 30 \\ 35 \\ 40 \\ 45 \end{pmatrix} \qquad T = \begin{pmatrix} 20 \\ 25 \\ 30 \\ 40 \\ 45 \\ 50 \\ 55 \\ 60 \\ 65 \end{pmatrix}$$

2.3 Calculation of Reynolds numbers according to AJ Arvia and JSW Carrozza, Mass Transfer in the Electrolysis of CuSO4-H2SO4 in Aqueous Solutions under Limiting Current Density and Forced Convection Employing a Cylindrical Cell with Rotating Electrodes, Electrochimica Acta, **1962**, pp. 65-78

The anode is the *inner* and *rotating* electrode. Therefore the chatacteristic length is D2 in Arvia et al.'s study and D2 is equal to "di" in this thesis. Arvia et al's. electrolyte composition: CuSO4, 1.5 - 3.5g/L; H2SO4, 147 g/L; Temperature 18C and RPM from 0 - 300.

$$ReArvia_i := \frac{U_i \cdot di}{\nu_i}$$

$$ReArvia = \begin{pmatrix} 48 \\ 53 \\ 91 \\ 150 \\ 205 \\ 270 \\ 340 \\ 422 \\ 520 \end{pmatrix} \quad RPM = \begin{pmatrix} 10 \\ 10 \\ 15 \\ 20 \\ 25 \\ 30 \\ 35 \\ 40 \\ 45 \end{pmatrix} \quad T = \begin{pmatrix} 20 \\ 25 \\ 30 \\ 40 \\ 45 \\ 50 \\ 55 \\ 60 \\ 65 \end{pmatrix}$$

2.4 Calculation of Reynolds numbers according to Barkey et al., J. Electrochem. Soc., Vol. 136, 8, **1989**, 2199-2207 and Silverman DC. *The Rotating Cylinder Electrode for Examining Velocity-Sensitive Corrosion - a Review*. Corrosion **2004**;60(11):1003-1022: Re=w*d^2/ν

$$ReSilverman_i := \frac{\omega_i \, di^2}{\nu_i} *$$

$$ReSilverman = \begin{pmatrix} 96 \\ 107 \\ 182 \\ 300 \\ 409 \\ 539 \\ 679 \\ 844 \\ 1040 \end{pmatrix} * \quad RPM = \begin{pmatrix} 10 \\ 10 \\ 15 \\ 20 \\ 25 \\ 30 \\ 35 \\ 40 \\ 45 \end{pmatrix} \quad T = \begin{pmatrix} 20 \\ 25 \\ 30 \\ 40 \\ 45 \\ 50 \\ 55 \\ 60 \\ 65 \end{pmatrix}$$

2.5 Calculation of Reynolds numbers according to H. Schlichting, Boundary-Layer Theory, **1968**, pp. 500-503.

$$ReSchlichting_i := U_i \cdot \frac{ro - ri}{\nu_i}$$

$$ro - ri = 0.032000m$$

$$ReSchlichting = \begin{pmatrix} 128 \\ 143 \\ 242 \\ 400 \\ 546 \\ 719 \\ 906 \\ 1125 \\ 1387 \end{pmatrix} \quad RPM = \begin{pmatrix} 10 \\ 10 \\ 15 \\ 20 \\ 25 \\ 30 \\ 35 \\ 40 \\ 45 \end{pmatrix} \quad T = \begin{pmatrix} 20 \\ 25 \\ 30 \\ 40 \\ 45 \\ 50 \\ 55 \\ 60 \\ 65 \end{pmatrix}$$

2.6 Calculation of Reynolds numbers according to Wang, L., et al., Chemical Engineering Science, 60, **2005**, 5555-5568 in Reapperance of Azimuthal Waves in Turbulent Taylor-Couette Flow at Large Aspect Ratio. Re=w*ri*d/ν

$$ReWang_i := \frac{\omega_i \cdot ri \cdot d}{\nu_i}$$

$$ReWang = \begin{pmatrix} 128 \\ 143 \\ 242 \\ 400 \\ 546 \\ 719 \\ 906 \\ 1125 \\ 1387 \end{pmatrix} \quad RPM = \begin{pmatrix} 10 \\ 10 \\ 15 \\ 20 \\ 25 \\ 30 \\ 35 \\ 40 \\ 45 \end{pmatrix} \quad T = \begin{pmatrix} 20 \\ 25 \\ 30 \\ 40 \\ 45 \\ 50 \\ 55 \\ 60 \\ 65 \end{pmatrix}$$

2.7 Comparison of Reynolds numbers for the RCE

It has been shown that:

ReNewman = ReGabe = ReEisenberg = ReArvia
ReSilverman = Re Barkey, and
ReSchilichting = ReWang

It appears that the equation for the Reynolds number used by Newman, Gabe, Eisenberg and Arvia is more often quoted in the literature than those used by Barkey, Silverman and Schlichting. Therefore the Reynolds equation used by Newman (Re=ω*d/2ν), Gabe, Eisenberg and Arvia will be used in this thesis.

$$Reynolds_i := ReNewman_i$$

2.8 Calculation of Reynolds numbers at Electrowinning and Electrorefining Temperatures and at Different Speeds fo Rotation

Reynolds Number at 25 C

$$Reynolds25 := \frac{\omega di^2}{(2\nu)_1} *$$

$$Reynolds25 = \begin{pmatrix} 53 \\ 53 \\ 80 \\ 107 \\ 134 \\ 160 \\ 187 \\ 214 \\ 241 \end{pmatrix} * \quad RPM = \begin{pmatrix} 10 \\ 10 \\ 15 \\ 20 \\ 25 \\ 30 \\ 35 \\ 40 \\ 45 \end{pmatrix}$$

Reynolds number at 45 C

$$Reynolds45 := \frac{\omega di^2}{(2\nu)_4} *$$

$$Reynolds45 = \begin{pmatrix} 82 \\ 82 \\ 123 \\ 164 \\ 205 \\ 246 \\ 287 \\ 328 \\ 369 \end{pmatrix} *$$

Reynolds Number at 50 C

$$\text{Reynolds50} := \frac{\omega \text{di}^2}{(2\nu)_5} *$$

$$\text{Reynolds50} = \begin{pmatrix} 90 \\ 90 \\ 135 \\ 180 \\ 225 \\ 270 \\ 315 \\ 359 \\ 404 \end{pmatrix} * \qquad \text{RPM} = \begin{pmatrix} 10 \\ 10 \\ 15 \\ 20 \\ 25 \\ 30 \\ 35 \\ 40 \\ 45 \end{pmatrix}$$

Reynolds Number at 65 C

$$\text{Reynolds65} := \frac{\omega \text{di}^2}{(2\nu)_8} *$$

$$\text{Reynolds65} = \begin{pmatrix} 116 \\ 116 \\ 173 \\ 231 \\ 289 \\ 347 \\ 405 \\ 462 \\ 520 \end{pmatrix} *$$

The Reynolds numbers at 25 rpm increases from Re= 134 at 25C to 205 at 45C, to 225 at 50C and to 289 at 65C. According to DR Gabe, Rotating Electrodes for Use in Electrodeposition Process Control, Plating and Surface Finishing, V 9, 1995, pp. 69-76, the critical Reynolds number for a RCE is 200.

2.8 Calculation of Taylor numbers According to J.Newman, Electrochemical Systems, 1991.

J. Newman (cited above) stated that turbulent flow prevails for Reynolds numbers greater than 3960 or Taylor numbers greater than about 3 x 10^6.

$$\text{TaNewman}_i := \left(\text{Reynolds}_i\right)^2 \cdot \frac{\text{ro} - \text{ri}}{\text{ri}}$$

$$\text{TaNewman} = \begin{pmatrix} 12248 \\ 15251 \\ 43972 \\ 120007 \\ 223537 \\ 387612 \\ 614949 \\ 949181 \\ 1443508 \end{pmatrix} \qquad \text{RPM} = \begin{pmatrix} 10 \\ 10 \\ 15 \\ 20 \\ 25 \\ 30 \\ 35 \\ 40 \\ 45 \end{pmatrix} \qquad \text{T} = \begin{pmatrix} 20 \\ 25 \\ 30 \\ 40 \\ 45 \\ 50 \\ 55 \\ 60 \\ 65 \end{pmatrix}$$

Taylor numbers at 25 rpm and 45C and 65C TaNewmanXXYY: XX=rpm and YY=temperature

$$TaNewman2545C := \left(\frac{\omega_4 \cdot di^2}{2\nu_4}\right)^2 \cdot \frac{ro - ri}{ri} \qquad TaNewman2545C = 224 \times 10^3$$

$$TaNewman2565C := \left(\frac{\omega_4 \cdot di^2}{\nu_8}\right)^2 \cdot \frac{ro - ri}{ri} \qquad TaNewman2565C = 2 \times 10^6$$

2.9 Calculation of Taylor number according to H. Schlichting, Boundary-Layer Theory, 1968, pp. 500-503.

H. Schlichting stated that for 41.3 < Ta < 400 Taylor vortices prevails between 41.3 and 400. Ta > 400 is turbulent.

$$TaSchlichting_i := U_i \frac{ro - ri}{\nu_i} \cdot \sqrt{\frac{ro - ri}{ri}} *$$

$$TaSchlichting = \begin{pmatrix} 295 \\ 329 \\ 559 \\ 924 \\ 1261 \\ 1660 \\ 2091 \\ 2598 \\ 3204 \end{pmatrix} * \qquad RPM = \begin{pmatrix} 10 \\ 10 \\ 15 \\ 20 \\ 25 \\ 30 \\ 35 \\ 40 \\ 45 \end{pmatrix} \qquad T = \begin{pmatrix} 20 \\ 25 \\ 30 \\ 40 \\ 45 \\ 50 \\ 55 \\ 60 \\ 65 \end{pmatrix}$$

Taylor number at 25rpm and 45 C TaSchlichtingXXYY: XX=rpm and YY=temperature

$$TaSchlichting2545 := U_4 \frac{ro - ri}{\nu_4} \cdot \sqrt{\frac{ro - ri}{ri}} * \qquad TaSchlichting2545 = 1.261 \times 10^3 *$$

Taylor number at 25rpm and 65 C

$$TaSchlichting2565 := U_4 \frac{ro - ri}{\nu_8} \cdot \sqrt{\frac{ro - ri}{ri}} * \qquad TaSchlichting2565 = 1.780 \times 10^3 *$$

ν with the subscripts of 4 and 8 indicate the kinematic viscosity at 45C and 65C, respectively.

2.10 SUMMARY

Schlichting (10) indicates that at Re = 94.5 and Ta 41.3 the flow is laminar and at the onset of vortex formation. It remains laminar up to ReSchlichting = 868 and TaSchlichting = 387. Since ReSchlichting and TaSchlichting at 25rpm and 45C and 65C are greater than 868 and 387, respectively; it has then been shown that the fluid flow for the RCE used in this thesis is turbulent according to Schlichting. However, Silverman (cited in Section 2.4 above) states that the Taylor number defined by Schlichting appears to be valid for narrow distances between the concentric cylinders (annular gap) only, i.e., 0.588mm.

The fluid flow for wider annular gaps such as used in this work (d=3.2cm) appears to be better described by Reynolds and Taylor numbers described by J. Newman, Electrochemical Systems, 1991. Newmand states that the fluid flow becomes instable at Re and Ta greater than 200 and 1708, respectively. It is therefore concluded that the fluid flow at the RCE is laminar with vortices since ReNewman at 25 rpm and 45C and 65C are 205 and 289, respectively. The TaylorNewman at 45C and 65C are 223,537 and 1.78 x 10^6, respectively. The onset of turbulence is at Ta 3 x 10^6 according to J. Newman.

3. CALCULATION OF THE LIMITING CURRENT DENSITY (iL) ACCORDING TO M. EISENBERG ET AL. AND J. NEWMAN CITED ABOVE.

3.1 Calculation of the Limiting Current Density According to J. Newman (Electrochemical Systems, 2004, pp. 398) when dR (rotating) = di (limiting CD electrode). The original equation was derived by Eisenberg et al. cited above.

$$iL_i := 0.0791 \cdot \left[n \cdot F \cdot D_i \frac{Co}{di} \cdot \left(\frac{\omega_i \cdot di^2}{2 \nu_i} \right)^{0.7} \left(Sc_i \right)^{0.356} \right] *$$

$$iL = \begin{pmatrix} 11 \\ 12 \\ 19 \\ 28 \\ 36 \\ 45 \\ 54 \\ 64 \\ 75 \end{pmatrix} \frac{mA}{cm^2} * \qquad Reynolds = \begin{pmatrix} 48 \\ 53 \\ 91 \\ 150 \\ 205 \\ 270 \\ 340 \\ 422 \\ 520 \end{pmatrix} \qquad T = \begin{pmatrix} 20 \\ 25 \\ 30 \\ 40 \\ 45 \\ 50 \\ 55 \\ 60 \\ 65 \end{pmatrix}$$

The diffusion layer thickness, δ

$$\delta Newman_i := \frac{n \cdot F \cdot Co \cdot D_i}{iL_i} *$$

$$\delta Newman = \begin{pmatrix} 613 \\ 624 \\ 472 \\ 388 \\ 333 \\ 293 \\ 264 \\ 239 \\ 219 \end{pmatrix} \mu m *$$

3.4 Calculation of the Limiting Current Density and Diffusion Layer Thickness Using Arvia et al.'s Equation cited above

$$iLArvia_i := 0.0791\left(\frac{di}{\nu_i}\right)^{-0.30}\cdot\left(U_i\right)^{0.70}\cdot\left(\frac{do}{di}\right)\cdot\left(Sc_i\right)^{-0.644}\cdot n\cdot F\cdot Co$$

$$iLArvia = \begin{pmatrix}68\\78\\117\\178\\229\\284\\341\\405\\474\end{pmatrix}\frac{mA}{cm^2} \qquad Reynolds = \begin{pmatrix}48\\53\\91\\150\\205\\270\\340\\422\\520\end{pmatrix} \qquad RPM = \begin{pmatrix}10\\10\\15\\20\\25\\30\\35\\40\\45\end{pmatrix} \qquad T = \begin{pmatrix}20\\25\\30\\40\\45\\50\\55\\60\\65\end{pmatrix}$$

SUMMARY
The DLT obtained from Eisenberg's equation is relatively higher than that obtained from Arvia's Equation. The Eisenberg Eq. was determined using hexacyanoferrate (II) and hexacyanoferrate (III) in 2M NaOH as supporting electrolyte. Arvia et al. obtained it using 1.5-3.5g/L copper in 1.5M sulfuric acid and also worked with a fixed cathode as the outer cylinder and a *stirred anode as the inner cylinder*.

3.6 Calculation of the Diffusion Layer Thickness at 10 and 25RPM and 45C and 64C Using Arvia's LCD and Nernst Equation.

$$\delta Arvia_i := \frac{n\cdot F\cdot Co\cdot D_i}{iLArvia_i}*$$

$$\delta Arvia = \begin{pmatrix}97\\98\\75\\61\\53\\46\\42\\38\\35\end{pmatrix}\mu m \qquad RPM = \begin{pmatrix}10\\10\\15\\20\\25\\30\\35\\40\\45\end{pmatrix} \qquad T = \begin{pmatrix}20\\25\\30\\40\\45\\50\\55\\60\\65\end{pmatrix}$$

3.7 Calculation of Diffusion Layer Thickness at 10RPM AND 45C. The results of the LCD and δ are plotted in Figure 3.

$$iLArvia1045 := 0.0791\left(\frac{di}{\nu_4}\right)^{-0.30}\cdot\left(U_1\right)^{0.70}\cdot\left(\frac{do}{di}\right)\cdot\left(Sc_4\right)^{-0.644}\cdot n\cdot F\cdot Co \qquad iLArvia1045 = 1204\,\frac{A}{m^2}$$

$$\delta Arvia1045 := \frac{n\cdot F\cdot Co\cdot D_4}{iLArvia1045}* \qquad \delta Arvia1045 = 100\,\mu m$$

3.8 Calculation of Diffusion Layer Thickness at 10RPM and 65C

$$iLArvia1065 := 0.0791\left(\frac{di}{\nu_8}\right)^{-0.30}\cdot\left(U_1\right)^{0.70}\cdot\left(\frac{do}{di}\right)\cdot\left(Sc_8\right)^{-0.644}\cdot n\cdot F\cdot Co \qquad iLArvia1065 = 1655\,\frac{A}{m^2}$$

$$\delta Arvia1065 := \frac{n\cdot F\cdot Co\cdot D_8}{iLArvia1065}* \qquad \delta Arvia1065 = 99\,\mu m$$

3.9 Calculation of Diffusion Layer Thickness at 25RPM and 45C

$$iLArvia2545 := 0.0791\left(\frac{di}{\nu_4}\right)^{-0.30}\cdot\left(U_4\right)^{0.70}\cdot\left(\frac{do}{di}\right)\cdot\left(Sc_4\right)^{-0.644}\cdot n\cdot F\cdot Co \qquad iLArvia2545 = 2286\,\frac{A}{m^2}$$

$$\delta Arvia2545 := \frac{n\cdot F\cdot Co\cdot D_4}{iLArvia2545}* \qquad \delta Arvia2545 = 53\,\mu m \qquad iLArvia_4 = 2286\,\frac{A}{m^2}$$

3.10 Calculation of Diffusion Layer Thickness at 25RPM and 65C

$$iLArvia2564 := 0.0791\left(\frac{di}{\nu_8}\right)^{-0.30}\cdot\left(U_4\right)^{0.70}\cdot\left(\frac{do}{di}\right)\cdot\left(Sc_8\right)^{-0.644}\cdot n\cdot F\cdot Co \qquad iLArvia2564 = 3143\,\frac{A}{m^2}$$

$$\delta Arvia2564 := \frac{n\cdot F\cdot Co\cdot D_8}{iLArvia2564}* \qquad \delta Arvia2564 = 52\,\mu m$$

3.9 Comparison of Limiting Current Densities

iL = iLNewman = iLEisenberg = ILGabe

$$iL = \begin{pmatrix} 107 \\ 123 \\ 185 \\ 282 \\ 361 \\ 448 \\ 539 \\ 639 \\ 749 \end{pmatrix} \frac{A}{m^2} \qquad RPM = \begin{pmatrix} 10 \\ 10 \\ 15 \\ 20 \\ 25 \\ 30 \\ 35 \\ 40 \\ 45 \end{pmatrix} \qquad T = \begin{pmatrix} 20 \\ 25 \\ 30 \\ 40 \\ 45 \\ 50 \\ 55 \\ 60 \\ 65 \end{pmatrix} \qquad iLArvia = \begin{pmatrix} 677 \\ 777 \\ 1174 \\ 1784 \\ 2286 \\ 2836 \\ 3415 \\ 4047 \\ 4742 \end{pmatrix} \frac{A}{m^2}$$

SUMMARY
The LCD data obtained from the Eq. of Eisenberg et al. is lower than that obtained from the Arvia et al. Eq. The equation for the LCD (iL) was obtained using hexacyanoferrate (II) and hexacyanoferrate (III) in 2M NaOH at 25C. Howeve, LCD iLArvia was obtained using 1.5-3.5g/L cupric ions and 1.5M sulfuric acid at 18C and the *rotating* electrode was the *anode* operating as *inner electrode*. This electrode set up is opposite to that used for this thesis.

Moreover, the diffusion coeficient for cupric ions for Arvia's study was 5.22 x 10^-6 cm^2/s and the kinematic viscosity was 1.279 x 10^-2 cm^2/s at 18C. These overall conditions do not exactly replicate to the conditions under which the data for this thesis were obtained. Therefore, Arvia's data will be used as a reference only.

4.0 Experimental Limiting Current Density and Diffusion Layer Thickness at 0, 10 and 25rpm and 45C and 65C

This experimental LCD was sourced from Chapter 3 - Section 3.2.3 - Table 3.2 to calculate the experimental diffusion layer thickness. The LCD data and δ results are plotted in Figure 3.

4.1 DLT at Zero RPM (Free Convection) at 45C and 65C

iLXXYY, XX=RPM and YY=temperature.

$iL0045 := 1037 \frac{A}{m^2}$ $\qquad \delta 0045 := n \cdot F \cdot Co \cdot \frac{D_4}{iL004}$ $\qquad \delta 0045 = 116 micron$

$iL0065 := 1432 \frac{A}{m^2}$ $\qquad \delta 0065 := n \cdot F \cdot Co \cdot \frac{D_8}{iL006}$ $\qquad \delta 0065 = 115 \mu m$

4.2 DLT at 10 RPM at 45C and 65C

$iL1045 := 1118 \frac{A}{m^2}$ $\qquad \delta 1045 := n \cdot F \cdot Co \cdot \frac{D_4}{iL104}$ $\qquad \delta 1045 = 108 \mu m$

$iL1065 := 1497 \frac{A}{m^2}$ $\qquad \delta 1065 := n \cdot F \cdot Co \cdot \frac{D_8}{iL106}$

$\delta 1065 = 110\,\mu m$

4.3 DLT at 25 RPM at 45C and 65C

$iL2545 := 1150\frac{A}{m^2}$ $\quad \delta 2545 := n \cdot F \cdot Co \cdot \frac{D_4}{iL2545}$ $\quad \delta 2545 = 105\,micron$

$iL2565 := 1660\frac{A}{m^2}$ $\quad \delta 2565 := n \cdot F \cdot Co \cdot \frac{D_8}{iL2565}$ $\quad \delta 2565 = 99\,micron$

Table 2: summarizes the calculated (using Arvia et al.'s equation) and the experimental diffusion layer thickness

TABLE 2

Calculated and Experimental Diffusion Layer Thickness at 0, 10 and 25 RPM and 45C and 65C

			Calculated		Experimental	
	RPM	Temp. C	DiffLT, μm	LCD	DiffLT, μm	LCD
Result :=						

	0	1	2	3	4	5
0	0	45	0	0	97	$1.037 \cdot 10^3$
1	0	65	0	0	115	$1.432 \cdot 10^3$
2	10	45	94	$1.07 \cdot 10^3$	90	$1.118 \cdot 10^3$
3	10	65	99	$1.655 \cdot 10^3$	110	$1.497 \cdot 10^3$
4	25	45	49	$2.032 \cdot 10^3$	87	$1.15 \cdot 10^3$
5	25	65	52	$3.143 \cdot 10^3$	99	$1.66 \cdot 10^3$

$j := 0..5$ $\quad RPMData := Result^{\langle 0 \rangle}$ $\quad TempData := Result^{\langle 1 \rangle}$ $\quad ExpDiffLT := (Result \cdot micron)^{\langle 4 \rangle}$

$DiffLT := (Result \cdot micron)^{\langle 2 \rangle}$ $\quad LCD := \left(Result \cdot \frac{A}{m^2}\right)^{\langle 3 \rangle}$ $\quad ExpLCD := \left(Result \cdot \frac{A}{m^2}\right)^{\langle 5 \rangle}$

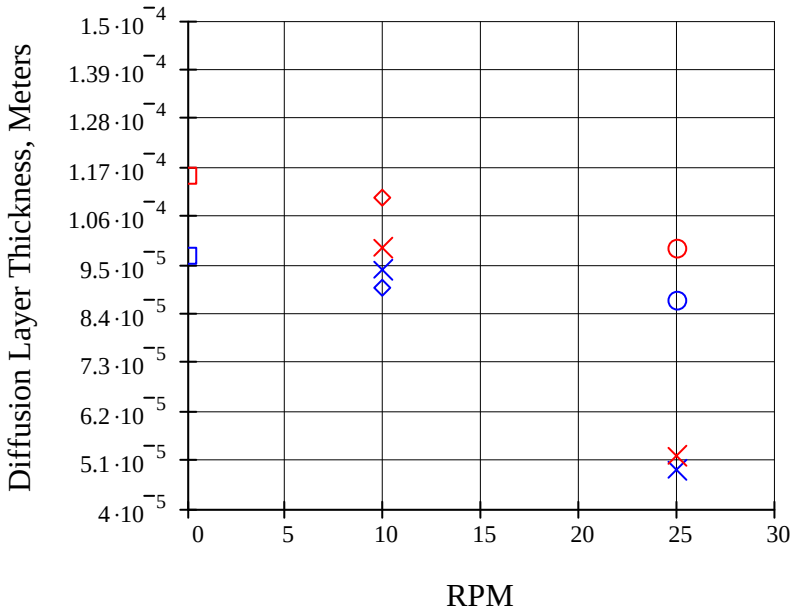

Figure 3: Calculated and Experimental Diffusion Layer Thickness at 0, 10 and 25 RPM and 45C and 65C

Legend: blue=45C; red=65C; squares=Free Convection; x = calculated using Arvia et al.'s LCD Eq. and Nernst Eq.

REFERENCES

1. Price D, Davenport W. *Physico-Chemical Properties of Copper Electrorefining and Electrowinning Electrolytes*. Metallurgical & Materials Transactions B-Process Metallurgy & Materials Processing Science 1981;12B:639-643.

2. Uceda D. Determination of Mass Transfer Characteristics in the Electrolysis of Copper [PhD Thesis]. Missouri-Rolla: University Missouri-Rolla; 1988.

3. Dutra A, O'Keefe T. *Copper Nucleation on Titanium for Thin Film Applications*. Journal of Applied Electrochemistry 1999;29:1217-1227.

4. Newman J, Thomas-Alyea KE. *Electrochemical Systems*. Third ed. Hoboken, New Jersey: John Wiley & Sons, Inc.; 2004.

5. Gabe D. *Rotating Electrodes for Use in Electrodeposition Process Control*. Plating & Surface Finishing 1995;9:69-76.

6. Eisenberg M, Tobias C, Wilke C. *Ionic Mass Transfer and Concentration Polarization at Rotating Electrodes*. Journal of the Electrochemical Society 1954;101(6):306-319.

7. Arvia AJ, Carrozza JSW. *Mass Transfer in the Electrolysis of Cuso4-H2so4 in Aqueous Solutions under Limiting Current and Forced Convection Employing a Cylindrical Cell with Rotating Electrodes*. Electrochimica Acta 1962;7:65-78.

8. Barkey D, Muller R, Tobias C. *Roughness Development in Metal Electrodeposition I. Experimental Results*. Journal of the Electrochemical Society 1989;138(8):2199-2207.

9. Silverman DC. *The Rotating Cylinder Electrode for Examining Velocity-Sensitive Corrosion - a Review*. Corrosion 2004;60(11):1003-1022.

10. Schlichting H. *Boundary-Layer Theory*. Sydney: McGraw-Hill; 1968.

11. Wang L, Olsen M, Vigil R. *Reappearance of Azimuthal Waves in Turbulent Taylor-Couette Flow at Large Aspect Ratio*. Chemical Engineering Science 2005;60:5555-5568.

12. Newman J. *Electrochemical Systems*. Second ed. London: Prentice-Hall International; 1991.

APPENDIX A - PART 2
FLUID FLOW AT LARGE ROTATING CYLINDER ELECTRODE

Mathcad 12 (2005) was used to undertake all the calculations shown in this Appendix. This program firstly calculates the kinematic viscosity and diffusion coefficient of cupric ions at different temperatures from the raw data collected from the literature (Ref. 1-4). It then derives the Reynolds and Taylor numbers to charaterize the fluid flow at the small and large RCE. Finally it uses these numbers to calculate the limiting current density and diffusion layer thickness, δ. The calculated limiting current density and δ are then compared with the experimental data.

The following table provides the raw data from the literature. An exponential curve was fitted to the raw data to obtain the absolute viscosity and diffusion of cupric ions data at the temperatures of interest.

TABLE 1

Temperature C	Fitted-Data Absolute Viscosity μ	Original Density Data(1)*, ρ	Fitted-Data Diffusion Coefficient Cupric Ions, D		Original Data (1)* Absolute Viscosity μodata	Original Data (2-4)* Diffusion Coefficient Cupric Ions DO
	$\frac{g}{cm\cdot s}$*	$\frac{g}{cm^3}$*	$\frac{cm^2}{s}$*	RPM*	$\frac{g}{cm\cdot s}$*	$\frac{cm^2}{s}$*

data :=

	0	1	2	3	4	5	6
0	20	0.019	1.186	$6\cdot10^{-6}$	10	0.019	$5\cdot10^{-6}$
1	25	0.017	1.183	$7\cdot10^{-6}$	10	0	$4.81\cdot10^{-6}$
2	30	0.015	1.18	$8\cdot10^{-6}$	15	0.015	$7.8\cdot10^{-6}$
3	40	0.012	1.174	$1\cdot10^{-5}$	20	0.012	$9.5\cdot10^{-6}$
4	45	0.011	1.173	$1.1\cdot10^{-5}$	25	0	$9.16\cdot10^{-6}$
5	50	$9.8\cdot10^{-3}$	1.168	$1.2\cdot10^{-5}$	30	$9.79\cdot10^{-3}$	0
6	55	$9.05\cdot10^{-3}$	1.165	$1.3\cdot10^{-5}$	35	0	$1\cdot10^{-5}$
7	60	$8.3\cdot10^{-3}$	1.161	$1.4\cdot10^{-5}$	40	$8.27\cdot10^{-3}$	0
8	65	$7.5\cdot10^{-3}$	1.15	$1.5\cdot10^{-5}$	45	0	$1.62\cdot10^{-5}$

$i := 0..8$*

$T := data^{\langle 0 \rangle}$*

$\mu := \left(data \cdot \frac{g}{cm\cdot s}\right)^{\langle 1 \rangle}$*

$\rho := \left(data \cdot \frac{g}{cm^3}\right)^{\langle 2 \rangle}$*

$D := \left(data \cdot \frac{cm^2}{s}\right)^{\langle 3 \rangle}$*

$RPM := data^{\langle 4 \rangle}$*

$\mu odata := \left(data \cdot \frac{g}{cm\cdot s}\right)^{\langle 5 \rangle}$*

$DO := \left(data \cdot \frac{cm^2}{s}\right)^{\langle 6 \rangle}$*

* References in brackets. The ZERO value in the Table 1 means NOT AVAILABLE data.

CALCULATION OF KINEMATIC VISCOSITY, μ/ρ (cm^2/s)

ν = kinematic viscosity - fitted data

$$\nu_i := \frac{\mu_i}{\rho_i} *$$

ν = kinematic viscosity - original data

$$N_i := \frac{\mu odata_i}{\rho_i} *$$

ν_i =

$1.573 \cdot 10^{-6}$	$m^2 \cdot s^{-1}$
$1.41 \cdot 10^{-6}$	
$1.246 \cdot 10^{-6}$	
$1.005 \cdot 10^{-6}$	
$9.207 \cdot 10^{-7}$	
$8.39 \cdot 10^{-7}$	
$7.772 \cdot 10^{-7}$	
$7.149 \cdot 10^{-7}$	
$6.522 \cdot 10^{-7}$	

T_i =

20
25
30
40
45
50
55
60
65

N_i =

0.01573	stokes
0	
0.01242	
0.01005	
0	
$8.38185 \cdot 10^{-3}$	
0	
$7.12317 \cdot 10^{-3}$	
0	

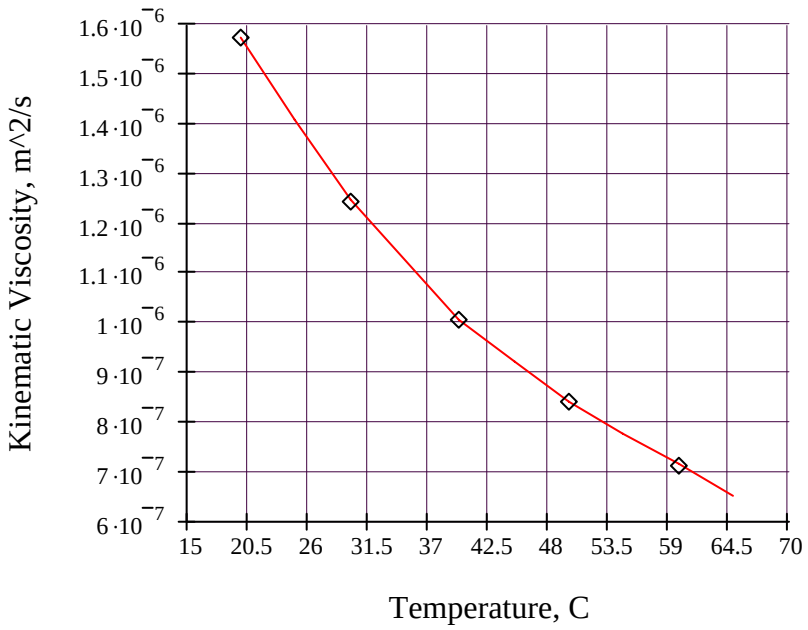

Figure 1. Plot of the Effect of Temperature on Kinematic Viscosity
Original Data (point) and Fitted Data (line)

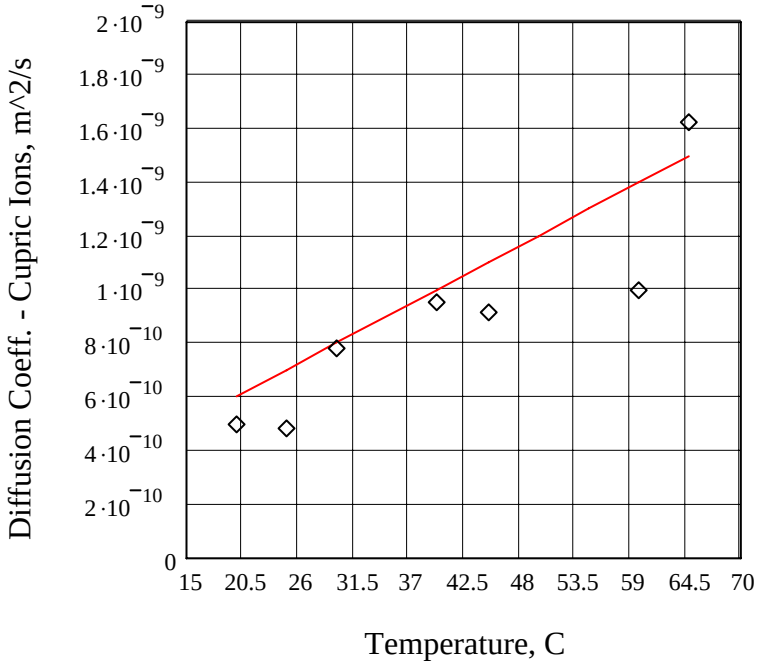

Figure 2. Plot on the Effect of Temperature on the Diffusion Coefficient of Cupric Ions
Original Data (point) and Fitted Data (line)

CALCULATION OF DIFFUSION LAYER THICKNESS USING THE NERNST EQUATION FOR THE SMALL RCE

$$Co := \frac{36 \cdot 10^{-3} \frac{mol}{cm^3}}{63.546} \quad n := 2 \quad F \equiv \frac{96485.3\,A \cdot s}{mol}$$

$di := 4.445\,cm$ di is the diameter of the inner RCE, the rotating electrode.

$do := 16.6\,cm$ do is the diameter of the outer RCE, stationary electrode.

$ri := \frac{di}{2}$ $ro := \frac{do}{2}$ $d := ro - ri$ d is the annulus, interelectrode distance

1. CALCULATION OF SCHMIDT NUMBERS, Sc

Sc numbers at their corresponding temperatures

$$Sc_i := \frac{\nu_i}{D_i}*$$

$$Sc = \begin{pmatrix} 2622 \\ 2014 \\ 1557 \\ 1005 \\ 837 \\ 699 \\ 598 \\ 511 \\ 435 \end{pmatrix} \quad T = \begin{pmatrix} 20 \\ 25 \\ 30 \\ 40 \\ 45 \\ 50 \\ 55 \\ 60 \\ 65 \end{pmatrix}$$

The Schmidt number varies from 435 at 65 degree C to 2736 at 20 degreeC.

2. CALCULATION OF REYNOLDS NUMBERS, Re

2.1 Calculation of Angular Velocity and Peripheral Velocity

Angular Velocity, ω

$$\omega_i := 2\pi \cdot \frac{RPM_i}{60 \cdot s}*$$

$$\omega = \begin{pmatrix} 1.047 \\ 1.047 \\ 1.571 \\ 2.094 \\ 2.618 \\ 3.142 \\ 3.665 \\ 4.189 \\ 4.712 \end{pmatrix} \frac{1}{sec}*$$

Peripheral Velocity, U

$$U_i := RPM_i \cdot \pi \cdot \frac{di}{60s}*$$

$$U = \begin{pmatrix} 2.327 \\ 2.327 \\ 3.491 \\ 4.655 \\ 5.818 \\ 6.982 \\ 8.146 \\ 9.31 \\ 10.473 \end{pmatrix} \frac{cm}{s}*$$

2.2 Calculation of Reynolds number according to J. Newman, Electrochemical Systems, **2004**, pp. 399: Re=d^2*ω/2ν ; DR Gabe and FC Walsh, J. App. Electrochemistry, 14, **1984**, pp. 555-564: Re=U*d/ν and Eisenberg, M, Tobias, and Wilke, C., J. Electrochem. Soc., **1954**, 101, 6, 306-319.

$$ReNewman_i := \frac{\omega_i \cdot di^2}{2 \cdot \nu_i} *$$

$$ReNewman = \begin{pmatrix} 658 \\ 734 \\ 1246 \\ 2058 \\ 2809 \\ 3699 \\ 4659 \\ 5788 \\ 7138 \end{pmatrix} * \quad RPM = \begin{pmatrix} 10 \\ 10 \\ 15 \\ 20 \\ 25 \\ 30 \\ 35 \\ 40 \\ 45 \end{pmatrix} \quad T = \begin{pmatrix} 20 \\ 25 \\ 30 \\ 40 \\ 45 \\ 50 \\ 55 \\ 60 \\ 65 \end{pmatrix}$$

$$ReGabe_i := U_i \cdot \frac{di}{\nu_i} *$$

$$ReGabe = \begin{pmatrix} 658 \\ 734 \\ 1246 \\ 2058 \\ 2809 \\ 3699 \\ 4659 \\ 5788 \\ 7138 \end{pmatrix} * \quad RPM = \begin{pmatrix} 10 \\ 10 \\ 15 \\ 20 \\ 25 \\ 30 \\ 35 \\ 40 \\ 45 \end{pmatrix} \quad T = \begin{pmatrix} 20 \\ 25 \\ 30 \\ 40 \\ 45 \\ 50 \\ 55 \\ 60 \\ 65 \end{pmatrix}$$

2.3 Calculation of Reynolds numbers according to AJ Arvia and JSW Carrozza, Mass Transfer in the Electrolysis of CuSO4-H2SO4 in Aqueous Solutions under Limiting Current Density and Forced Convection Employing a Cylindrical Cell with Rotating Electrodes, Electrochimica Acta, **1962**, pp. 65-78

The anode is the *inner* and *rotating* electrode. Therefore the chatacteristic length is D2 in Arvia et al.'s study and D2 is equal to "di" in this thesis. Arvia et al's. electrolyte composition: CuSO4, 1.5 - 3.5g/L; H2SO4, 147 g/L; Temperature 18C and RPM from 0 - 300.

$$ReArvia_i := \frac{U_i \cdot di}{\nu_i}$$

$$ReArvia = \begin{pmatrix} 658 \\ 734 \\ 1246 \\ 2058 \\ 2809 \\ 3699 \\ 4659 \\ 5788 \\ 7138 \end{pmatrix} \quad RPM = \begin{pmatrix} 10 \\ 10 \\ 15 \\ 20 \\ 25 \\ 30 \\ 35 \\ 40 \\ 45 \end{pmatrix} \quad T = \begin{pmatrix} 20 \\ 25 \\ 30 \\ 40 \\ 45 \\ 50 \\ 55 \\ 60 \\ 65 \end{pmatrix}$$

2.4 Calculation of Reynolds numbers according to Barkey et al., J. Electrochem. Soc., Vol. 136, 8, **1989**, 2199-2207 and Silverman DC. *The Rotating Cylinder Electrode for Examining Velocity-Sensitive Corrosion - a Review*. Corrosion **2004**;60(11):1003-1022: Re=w*d^2/ν

$$ReSilverman_i := \frac{\omega_i \cdot di^2}{\nu_i} *$$

$$ReSilverman = \begin{pmatrix} 1315 \\ 1467 \\ 2492 \\ 4116 \\ 5618 \\ 7398 \\ 9318 \\ 11577 \\ 14276 \end{pmatrix} * \quad RPM = \begin{pmatrix} 10 \\ 10 \\ 15 \\ 20 \\ 25 \\ 30 \\ 35 \\ 40 \\ 45 \end{pmatrix} \quad T = \begin{pmatrix} 20 \\ 25 \\ 30 \\ 40 \\ 45 \\ 50 \\ 55 \\ 60 \\ 65 \end{pmatrix}$$

2.5 Calculation of Reynolds numbers according to H. Schlichting, Boundary-Layer Theory, **1968**, pp. 500-503.

$$ReSchlichting_i := U_i \cdot \frac{ro - ri}{\nu_i}$$

$$ro - ri = 0.060775m$$

$$ReSchlichting = \begin{pmatrix} 899 \\ 1003 \\ 1703 \\ 2814 \\ 3841 \\ 5057 \\ 6370 \\ 7914 \\ 9760 \end{pmatrix} \quad RPM = \begin{pmatrix} 10 \\ 10 \\ 15 \\ 20 \\ 25 \\ 30 \\ 35 \\ 40 \\ 45 \end{pmatrix} \quad T = \begin{pmatrix} 20 \\ 25 \\ 30 \\ 40 \\ 45 \\ 50 \\ 55 \\ 60 \\ 65 \end{pmatrix}$$

2.6 Calculation of Reynolds numbers according to Wang, L., et al., Chemical Engineering Science, 60, **2005**, 5555-5568 in Reapperance of Azimuthal Waves in Turbulent Taylor-Couette Flow at Large Aspect Ratio. Re=w*ri*d/ν

$$ReWang_i := \frac{\omega_i \cdot ri \cdot d}{\nu_i}$$

$$ReWang = \begin{pmatrix} 899 \\ 1003 \\ 1703 \\ 2814 \\ 3841 \\ 5057 \\ 6370 \\ 7914 \\ 9760 \end{pmatrix} \quad RPM = \begin{pmatrix} 10 \\ 10 \\ 15 \\ 20 \\ 25 \\ 30 \\ 35 \\ 40 \\ 45 \end{pmatrix} \quad T = \begin{pmatrix} 20 \\ 25 \\ 30 \\ 40 \\ 45 \\ 50 \\ 55 \\ 60 \\ 65 \end{pmatrix}$$

2.7 Comparison of Reynolds numbers for the RCE

It has been shown that: ReNewman = ReGabe = ReEisenberg = ReArvia
ReSilverman = Re Barkey, and
ReSchilichting = ReWang

It appears that the equation for the Reynolds number used by Newman, Gabe, Eisenberg and Arvia is more often quoted in the literature than those used by Barkey, Silverman and Schlichting. Therefore the Reynolds equation used by Newman (Re=ω*d/2ν), Gabe, Eisenberg and Arvia will be used in this thesis.

$$Reynolds_i := ReNewman_i$$

2.8 Calculation of Reynolds numbers at Electrowinning and Electrorefining Temperatures and at Different Speeds fo Rotation

Reynolds Number at 25 C

$$Reynolds25 := \frac{\omega di^2}{(2\nu)_1} *$$

$$Reynolds25 = \begin{pmatrix} 734 \\ 734 \\ 1101 \\ 1467 \\ 1834 \\ 2201 \\ 2568 \\ 2935 \\ 3302 \end{pmatrix} * \qquad RPM = \begin{pmatrix} 10 \\ 10 \\ 15 \\ 20 \\ 25 \\ 30 \\ 35 \\ 40 \\ 45 \end{pmatrix}$$

Reynolds number at 45 C

$$Reynolds45 := \frac{\omega di^2}{(2\nu)_4} *$$

$$Reynolds45 = \begin{pmatrix} 1124 \\ 1124 \\ 1685 \\ 2247 \\ 2809 \\ 3371 \\ 3933 \\ 4494 \\ 5056 \end{pmatrix} *$$

Reynolds Number at 50 C

$$Reynolds50 := \frac{\omega di^2}{(2\nu)_5} *$$

$$Reynolds50 = \begin{pmatrix} 1233 \\ 1233 \\ 1849 \\ 2466 \\ 3082 \\ 3699 \\ 4315 \\ 4932 \\ 5548 \end{pmatrix} * \qquad RPM = \begin{pmatrix} 10 \\ 10 \\ 15 \\ 20 \\ 25 \\ 30 \\ 35 \\ 40 \\ 45 \end{pmatrix}$$

Reynolds Number at 65 C

$$Reynolds65 := \frac{\omega di^2}{(2\nu)_8} *$$

$$Reynolds65 = \begin{pmatrix} 1586 \\ 1586 \\ 2379 \\ 3173 \\ 3966 \\ 4759 \\ 5552 \\ 6345 \\ 7138 \end{pmatrix} *$$

The Reynolds numbers at 25 rpm increases from Re= 134 at 25C to 205 at 45C, to 225 at 50C and to 289 at 65C. According to DR Gabe, Rotating Electrodes for Use in Electrodeposition Process Control, Plating and Surface Finishing, V 9, 1995, pp. 69-76, the critical Reynolds number for a RCE is 200.

2.8 Calculation of Taylor numbers According to J.Newman, Electrochemical Systems, 1991.

J. Newman (cited above) stated that turbulent flow prevails for Reynolds numbers greater than 3960 or Taylor numbers greater than about 3 x 10^6.

$$TaNewman_i := \left(Reynolds_i\right)^2 \cdot \frac{ro - ri}{ri}$$

$$TaNewman = \begin{pmatrix} 1182262 \\ 1472126 \\ 4244500 \\ 11583817 \\ 21577247 \\ 37414810 \\ 59358842 \\ 91621151 \\ 139336753 \end{pmatrix} \qquad RPM = \begin{pmatrix} 10 \\ 10 \\ 15 \\ 20 \\ 25 \\ 30 \\ 35 \\ 40 \\ 45 \end{pmatrix} \qquad T = \begin{pmatrix} 20 \\ 25 \\ 30 \\ 40 \\ 45 \\ 50 \\ 55 \\ 60 \\ 65 \end{pmatrix}$$

Taylor numbers at 25 rpm and 45C and 65C TaNewmanXXYY: XX=rpm and YY=temperature

$$TaNewman2545C := \left(\frac{\omega_4 \cdot di^2}{2\nu_4}\right)^2 \cdot \frac{ro - ri}{ri} \qquad TaNewman2545C = 22 \times 10^6$$

$$TaNewman2565C := \left(\frac{\omega_4 \cdot di^2}{\nu_8}\right)^2 \cdot \frac{ro - ri}{ri} \qquad TaNewman2565C = 2 \times 10^8$$

2.9 Calculation of Taylor number according to H. Schlichting, Boundary-Layer Theory, 1968, pp. 500-503.

H. Schlichting stated that for 41.3 < Ta < 400 Taylor vortices prevails between 41.3 and 400. Ta > 400 is turbulent.

$$TaSchlichting_i := U_i \frac{ro - ri}{\nu_i} \cdot \sqrt{\frac{ro - ri}{ri}} *$$

$$TaSchlichting = \begin{pmatrix} 1487 \\ 1659 \\ 2817 \\ 4653 \\ 6351 \\ 8363 \\ 10534 \\ 13087 \\ 16139 \end{pmatrix} * \quad RPM = \begin{pmatrix} 10 \\ 10 \\ 15 \\ 20 \\ 25 \\ 30 \\ 35 \\ 40 \\ 45 \end{pmatrix} \quad T = \begin{pmatrix} 20 \\ 25 \\ 30 \\ 40 \\ 45 \\ 50 \\ 55 \\ 60 \\ 65 \end{pmatrix}$$

Taylor number at 25rpm and 45 C TaSchlichtingXXYY: XX=rpm and YY=temperature

$$TaSchlichting2545 := U_4 \frac{ro - ri}{\nu_4} \cdot \sqrt{\frac{ro - ri}{ri}} * \qquad TaSchlichting2545 = 6.351 \times 10^3 *$$

Taylor number at 25rpm and 65 C

$$TaSchlichting2565 := U_4 \frac{ro - ri}{\nu_8} \cdot \sqrt{\frac{ro - ri}{ri}} * \qquad TaSchlichting2565 = 8.966 \times 10^3 *$$

ν with the subscripts of 4 and 8 indicate the kinematic viscosity at 45C and 65C, respectively.

2.10 SUMMARY

Schlichting (10) indicates that at Re = 94.5 and Ta 41.3 the flow is laminar and at the onset of vortex formation. It remains laminar up to ReSchlichting = 868 and TaSchlichting = 387. Since ReSchlichting and TaSchlichting at 25rpm and 45C and 65C are greater than 868 and 387, respectively; it has then been shown that the fluid flow for the RCE used in this thesis is turbulent according to Schlichting. However, Silverman (cited in Section 2.4 above) states that the Taylor number defined by Schlichting appears to be valid for narrow distances between the concentric cylinders (annular gap) only, i.e., 0.588mm.

The fluid flow for wider annular gaps such as used in this work (d=3.2cm) appears to be better described by Reynolds and Taylor numbers described by J. Newman, Electrochemical Systems, 1991. Newmand states that the fluid flow becomes instable at Re and Ta greater than 200 and 1708, respectively. It is therefore concluded that the fluid flow at the RCE is laminar with vortices since ReNewman at 25 rpm and 45C and 65C are 205 and 289, respectively. The TaylorNewman at 45C and 65C are 223,537 and 1.78 x 10^6, respectively. The onset of turbulence is at Ta 3 x 10^6 according to J. Newman.

3. CALCULATION OF THE LIMITING CURRENT DENSITY (iL) ACCORDING TO M. EISENBERG ET AL. AND J. NEWMAN CITED ABOVE.

3.1 Calculation of the Limiting Current Density According to J. Newman (Electrochemical Systems, 2004, pp. 398) when dR (rotating) = di (limiting CD electrode). The original equation was derived by Eisenberg et al. cited above.

$$iL_i := 0.0791\left[n \cdot F \cdot D_i \frac{Co}{di} \cdot \left(\frac{\omega_i \cdot di^2}{2\nu_i}\right)^{0.7} \left(Sc_i\right)^{0.356}\right]*$$

$$iL = \begin{pmatrix} 18 \\ 21 \\ 31 \\ 48 \\ 61 \\ 76 \\ 91 \\ 108 \\ 126 \end{pmatrix} \frac{mA}{cm^2}* \qquad Reynolds = \begin{pmatrix} 658 \\ 734 \\ 1246 \\ 2058 \\ 2809 \\ 3699 \\ 4659 \\ 5788 \\ 7138 \end{pmatrix} \qquad T = \begin{pmatrix} 20 \\ 25 \\ 30 \\ 40 \\ 45 \\ 50 \\ 55 \\ 60 \\ 65 \end{pmatrix}$$

The diffusion layer thickness, δ

$$\delta Newman_i := \frac{n \cdot F \cdot Co \cdot D_i}{iL_i}*$$

$$\delta Newman = \begin{pmatrix} 363 \\ 369 \\ 280 \\ 230 \\ 197 \\ 174 \\ 156 \\ 142 \\ 130 \end{pmatrix} \mu m*$$

3.4 Calculation of the Limiting Current Density and Diffusion Layer Thickness Using Arvia et al.'s Equation cited above

$$iLArvia_i := 0.0791\left(\frac{di}{\nu_i}\right)^{-0.30} \cdot \left(U_i\right)^{0.70} \cdot \left(\frac{do}{di}\right) \cdot \left(Sc_i\right)^{-0.644} \cdot n \cdot F \cdot Co$$

$$iLArvia = \begin{pmatrix} 67 \\ 77 \\ 117 \\ 178 \\ 228 \\ 282 \\ 340 \\ 403 \\ 472 \end{pmatrix} \frac{mA}{cm^2} \qquad Reynolds = \begin{pmatrix} 658 \\ 734 \\ 1246 \\ 2058 \\ 2809 \\ 3699 \\ 4659 \\ 5788 \\ 7138 \end{pmatrix} \qquad RPM = \begin{pmatrix} 10 \\ 10 \\ 15 \\ 20 \\ 25 \\ 30 \\ 35 \\ 40 \\ 45 \end{pmatrix} \qquad T = \begin{pmatrix} 20 \\ 25 \\ 30 \\ 40 \\ 45 \\ 50 \\ 55 \\ 60 \\ 65 \end{pmatrix}$$

SUMMARY
The DLT obtained from Eisenberg's equation is relatively higher than that obtained from Arvia's Equation. The Eisenberg Eq. was determined using hexacyanoferrate (II) and hexacyanoferrate (III) in 2M NaOH as supporting electrolyte. Arvia et al. obtained it using 1.5-3.5g/L copper in 1.5M sulfuric acid and also worked with a fixed cathode as the outer cylinder and a *stirred anode as the inner cylinder*.

3.6 Calculation of the Diffusion Layer Thickness at 10 and 25RPM and 45C and 64C Using Arvia's LCD and Nernst Equation.

$$\delta Arvia_i := \frac{n \cdot F \cdot Co \cdot D_i}{iLArvia_i} * \qquad \delta Arvia = \begin{pmatrix} 97 \\ 99 \\ 75 \\ 62 \\ 53 \\ 46 \\ 42 \\ 38 \\ 35 \end{pmatrix} \mu m \qquad RPM = \begin{pmatrix} 10 \\ 10 \\ 15 \\ 20 \\ 25 \\ 30 \\ 35 \\ 40 \\ 45 \end{pmatrix} \qquad T = \begin{pmatrix} 20 \\ 25 \\ 30 \\ 40 \\ 45 \\ 50 \\ 55 \\ 60 \\ 65 \end{pmatrix}$$

3.7 Calculation of Diffusion Layer Thickness at 10RPM AND 45C. The results of the LCD and δ are plotted in Figure 3.

$$iLArvia1045 := 0.0791 \left(\frac{di}{\nu_4} \right)^{-0.30} \cdot \left(U_1 \right)^{0.70} \cdot \left(\frac{do}{di} \right) \cdot \left(Sc_4 \right)^{-0.644} \cdot n \cdot F \cdot Co \qquad iLArvia1045 = 1198 \frac{A}{m^2}$$

$$\delta Arvia1045 := \frac{n \cdot F \cdot Co \cdot D_4}{iLArvia1045} * \qquad \delta Arvia1045 = 100 \mu m$$

3.8 Calculation of Diffusion Layer Thickness at 10RPM and 65C

$$iLArvia1065 := 0.0791\left(\frac{di}{\nu_8}\right)^{-0.30}\cdot\left(U_1\right)^{0.70}\cdot\left(\frac{do}{di}\right)\cdot\left(Sc_8\right)^{-0.644}\cdot n\cdot F\cdot Co \qquad iLArvia1065 = 1648\,\frac{A}{m^2}$$

$$\delta Arvia1065 := \frac{n\cdot F\cdot Co\cdot D_8}{iLArvia1065^*} \qquad \delta Arvia1065 = 100\,\mu m$$

3.9 Calculation of Diffusion Layer Thickness at 25RPM and 45C

$$iLArvia2545 := 0.0791\left(\frac{di}{\nu_4}\right)^{-0.30}\cdot\left(U_4\right)^{0.70}\cdot\left(\frac{do}{di}\right)\cdot\left(Sc_4\right)^{-0.644}\cdot n\cdot F\cdot Co \qquad iLArvia2545 = 2276\,\frac{A}{m^2}$$

$$\delta Arvia2545 := \frac{n\cdot F\cdot Co\cdot D_4}{iLArvia2545^*} \qquad \delta Arvia2545 = 53\,\mu m \qquad iLArvia_4 = 2276\,\frac{A}{m^2}$$

3.10 Calculation of Diffusion Layer Thickness at 25RPM and 65C

$$iLArvia2564 := 0.0791\left(\frac{di}{\nu_8}\right)^{-0.30}\cdot\left(U_4\right)^{0.70}\cdot\left(\frac{do}{di}\right)\cdot\left(Sc_8\right)^{-0.644}\cdot n\cdot F\cdot Co \qquad iLArvia2564 = 3129\,\frac{A}{m^2}$$

$$\delta Arvia2564 := \frac{n\cdot F\cdot Co\cdot D_8}{iLArvia2564^*} \qquad \delta Arvia2564 = 52\,\mu m$$

3.9 Comparison of Limiting Current Densities

iL = iLNewman = iLEisenberg = ILGabe

$$iL = \begin{pmatrix} 181 \\ 207 \\ 313 \\ 476 \\ 609 \\ 756 \\ 910 \\ 1079 \\ 1264 \end{pmatrix}\frac{A}{m^2} \qquad RPM = \begin{pmatrix} 10 \\ 10 \\ 15 \\ 20 \\ 25 \\ 30 \\ 35 \\ 40 \\ 45 \end{pmatrix} \qquad T = \begin{pmatrix} 20 \\ 25 \\ 30 \\ 40 \\ 45 \\ 50 \\ 55 \\ 60 \\ 65 \end{pmatrix} \qquad iLArvia = \begin{pmatrix} 675 \\ 774 \\ 1168 \\ 1776 \\ 2276 \\ 2823 \\ 3400 \\ 4030 \\ 4721 \end{pmatrix}\frac{A}{m^2}$$

SUMMARY

The LCD data obtained from the Eq. of Eisenberg et al. is lower than that obtained from the Arvia et al. Eq. The equation for the LCD (iL) was obtained using hexacyanoferrate (II) and hexacyanoferrate (III) in 2M NaOH at 25C. Howeve, LCD iLArvia was obtained using 1.5-3.5g/L cupric ions and 1.5M sulfuric acid at 18C and the *rotating* electrode was the *anode* operating as *inner electrode*. This electrode set up is opposite to that used for this thesis.

Moreover, the diffusion coeficient for cupric ions for Arvia's study was 5.22 x 10^-6 cm^2/s and the kinematic viscosity was 1.279 x 10^-2 cm^2/s at 18C. These overall conditions do not exactly replicate to the conditions under which the data for this thesis were obtained. Therefore, Arvia's data will be used as a reference only.

4.0 Experimental Limiting Current Density and Diffusion Layer Thickness at 0, 10 and 25rpm and 45C and 65C

This experimental LCD was sourced from Chapter 3 - Section 3.2.3 - Table 3.2 to calculate the experimental diffusion layer thickness. The LCD data and δ results are plotted in Figure 3.

4.1 DLT at Zero RPM (Free Convection) at 45C and 65C

iLXXYY, XX=RPM and YY=temperature.

$iL0045 := 1037 \frac{A}{m^2}$ $\quad \delta 0045 := n \cdot F \cdot Co \cdot \frac{D_4}{iL0045}$ $\quad \delta 0045 = 116 micron$

$iL0065 := 1432 \frac{A}{m^2}$ $\quad \delta 0065 := n \cdot F \cdot Co \cdot \frac{D_8}{iL0065}$ $\quad \delta 0065 = 115 \mu m$

4.2 DLT at 10 RPM at 45C and 65C

$iL1045 := 1118 \frac{A}{m^2}$ $\quad \delta 1045 := n \cdot F \cdot Co \cdot \frac{D_4}{iL1045}$ $\quad \delta 1045 = 108 \mu m$

$iL1065 := 1497 \frac{A}{m^2}$ $\quad \delta 1065 := n \cdot F \cdot Co \cdot \frac{D_8}{iL1065}$ $\quad \delta 1065 = 110 \mu m$

4.3 DLT at 25 RPM at 45C and 65C

$iL2545 := 1150 \frac{A}{m^2}$ $\quad \delta 2545 := n \cdot F \cdot Co \cdot \frac{D_4}{iL2545}$ $\quad \delta 2545 = 105 micron$

$iL2565 := 1660 \frac{A}{m^2}$ $\quad \delta 2565 := n \cdot F \cdot Co \cdot \frac{D_8}{iL2565}$ $\quad \delta 2565 = 99 micron$

Table 2: summarizes the calculated (using Arvia et al.'s equation) and the experimental diffusion layer thickness

TABLE 2

Calculated and Experimental Diffusion Layer Thickness at 0, 10 and 25 RPM and 45C and 65C

			Calculated		Experimental	
	RPM	Temp. C	DiffLT, μm	LCD	DiffLT, μm	LCD
Result :=						
0	0	45	0	0	97	$1.037 \cdot 10^3$
1	0	65	0	0	115	$1.432 \cdot 10^3$
2	10	45	94	$1.07 \cdot 10^3$	90	$1.118 \cdot 10^3$
3	10	65	99	$1.655 \cdot 10^3$	110	$1.497 \cdot 10^3$
4	25	45	49	$2.032 \cdot 10^3$	87	$1.15 \cdot 10^3$
5	25	65	52	$3.143 \cdot 10^3$	99	$1.66 \cdot 10^3$

$j := 0..5$ $\quad RPMData := Result^{\langle 0 \rangle}$ $\quad TempData := Result^{\langle 1 \rangle}$ $\quad ExpDiffLT := (Result \cdot micron)^{\langle 4 \rangle}$

$DiffLT := (Result \cdot micron)^{\langle 2 \rangle}$ $\quad LCD := \left(Result \cdot \frac{A}{m^2} \right)^{\langle 3 \rangle}$ $\quad ExpLCD := \left(Result \cdot \frac{A}{m^2} \right)^{\langle 5 \rangle}$

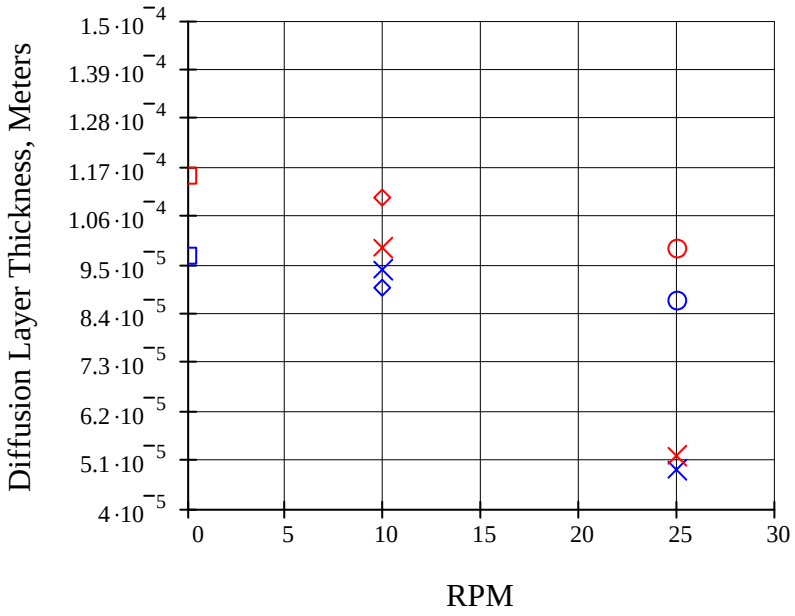

Figure 3: Calculated and Experimental Diffusion Layer Thickness at 0, 10 and 25 RPM and 45C and 65C

Legend: blue=45C; red=65C; squares=Free Convection; x = calculated using Arvia et al.'s LCD Eq. and Nernst Eq.

REFERENCES

1. Price D, Davenport W. *Physico-Chemical Properties of Copper Electrorefining and Electrowinning Electrolytes*. Metallurgical & Materials Transactions B-Process Metallurgy & Materials Processing Science 1981;12B:639-643.

2. Uceda D. Determination of Mass Transfer Characteristics in the Electrolysis of Copper [PhD Thesis]. Missouri-Rolla: University Missouri-Rolla; 1988.

3. Dutra A, O'Keefe T. *Copper Nucleation on Titanium for Thin Film Applications*. Journal of Applied Electrochemistry 1999;29:1217-1227.

4. Newman J, Thomas-Alyea KE. *Electrochemical Systems*. Third ed. Hoboken, New Jersey: John Wiley & Sons, Inc.; 2004.

5. Gabe D. *Rotating Electrodes for Use in Electrodeposition Process Control*. Plating & Surface Finishing 1995;9:69-76.

6. Eisenberg M, Tobias C, Wilke C. *Ionic Mass Transfer and Concentration Polarization at Rotating Electrodes*. Journal of the Electrochemical Society 1954;101(6):306-319.

7. Arvia AJ, Carrozza JSW. *Mass Transfer in the Electrolysis of Cuso4-H2so4 in Aqueous Solutions under Limiting Current and Forced Convection Employing a Cylindrical Cell with Rotating Electrodes*. Electrochimica Acta 1962;7:65-78.

8. Barkey D, Muller R, Tobias C. *Roughness Development in Metal Electrodeposition I. Experimental Results*. Journal of the Electrochemical Society 1989;138(8):2199-2207.

9. Silverman DC. *The Rotating Cylinder Electrode for Examining Velocity-Sensitive Corrosion - a Review*. Corrosion 2004;60(11):1003-1022.

10. Schlichting H. *Boundary-Layer Theory*. Sydney: McGraw-Hill; 1968.

11. Wang L, Olsen M, Vigil R. *Reappearance of Azimuthal Waves in Turbulent Taylor-Couette Flow at Large Aspect Ratio*. Chemical Engineering Science 2005;60:5555-5568.

12. Newman J. *Electrochemical Systems*. Second ed. London: Prentice-Hall International; 1991.

APPENDIX B

ELECTROCHEMICAL IMPEDANCE SPECTROCPY DATA USING GUAR AT -490mV vs. MSE AND 45^{o}C

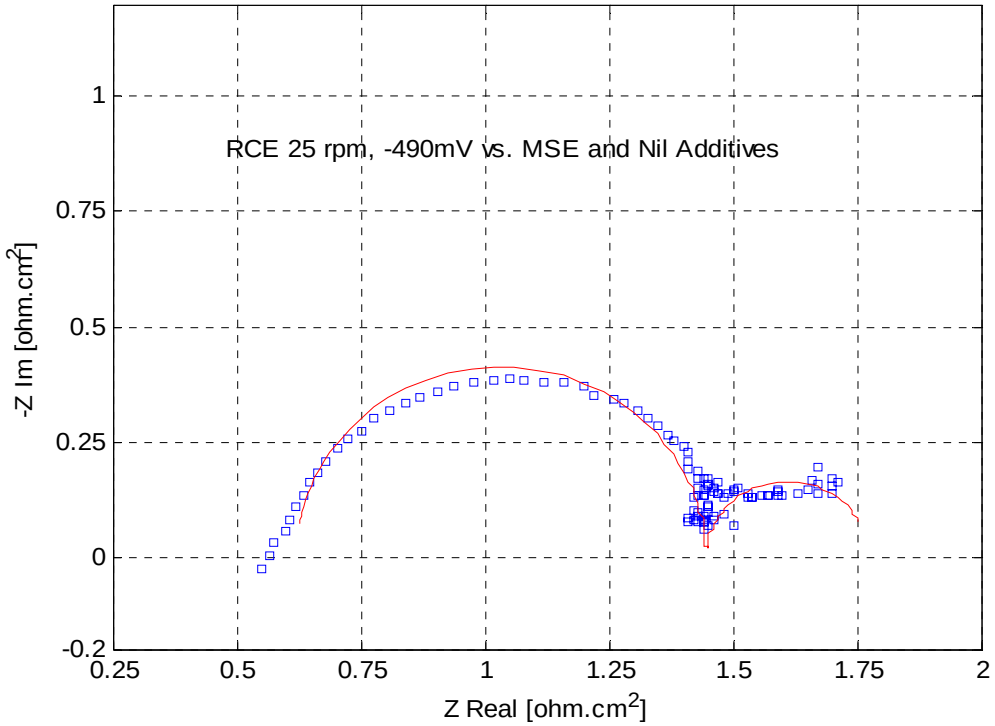

Figure 1: Complex-Plane Plot of Experimental and Simulated Impedance Spectra at 45^{o}C in the Absence of Guar at -490mV vs. MSE

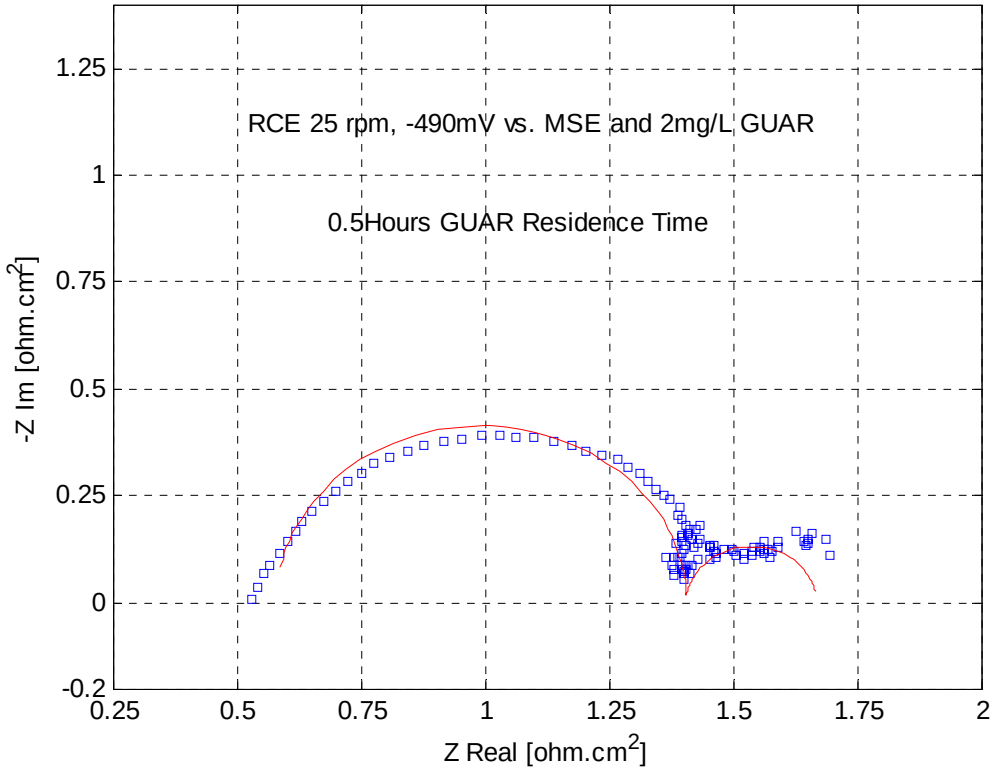

Figure 2: Complex-Plane Plot of Experimental and Simulated Impedance Spectra at 45^{o}C in the Presence of Guar at -490mV vs. MSE and 0.5Hours Residence Time

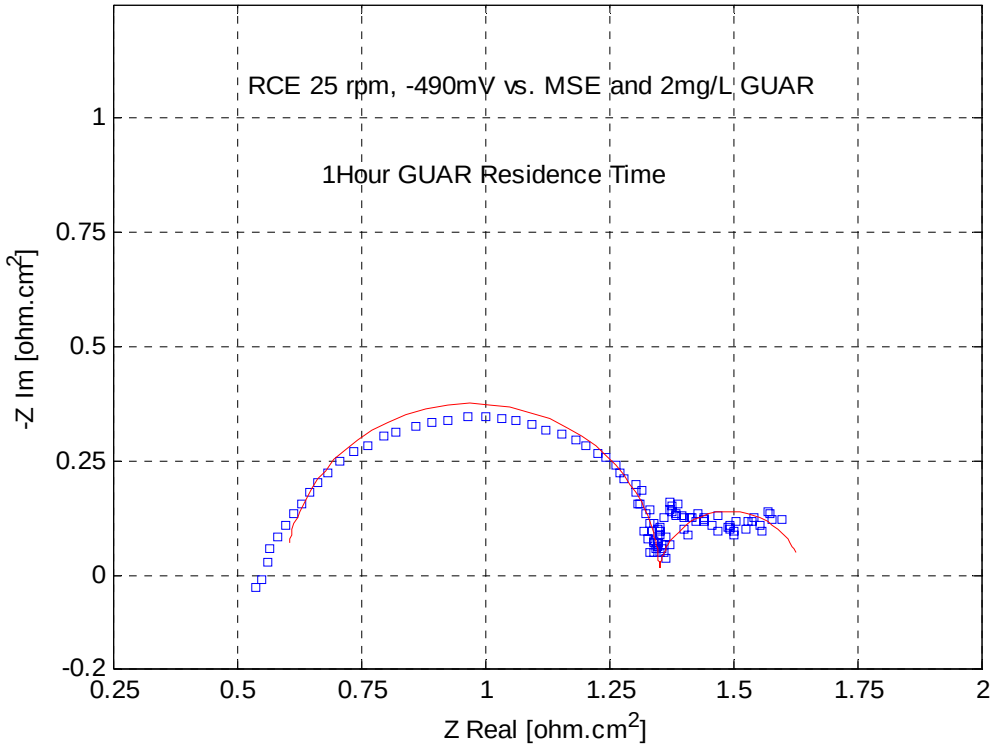

Figure 3: Complex-Plane Plot of Experimental and Simulated Impedance Spectra at 45°C in the Presence of Guar at -490mV vs. MSE and 1Hour Residence Time

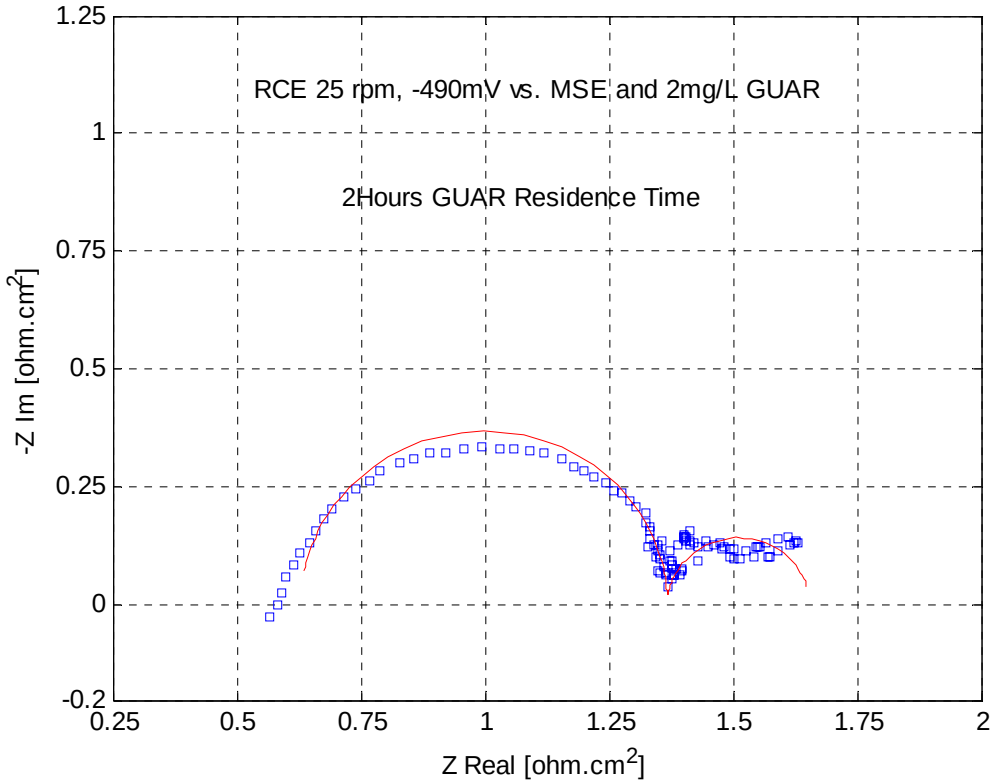

Figure 4: Complex-Plane Plot of Experimental and Simulated Impedance Spectra at 45°C in the Presence of Guar at -490mV vs. MSE and 2Hours Residence Time

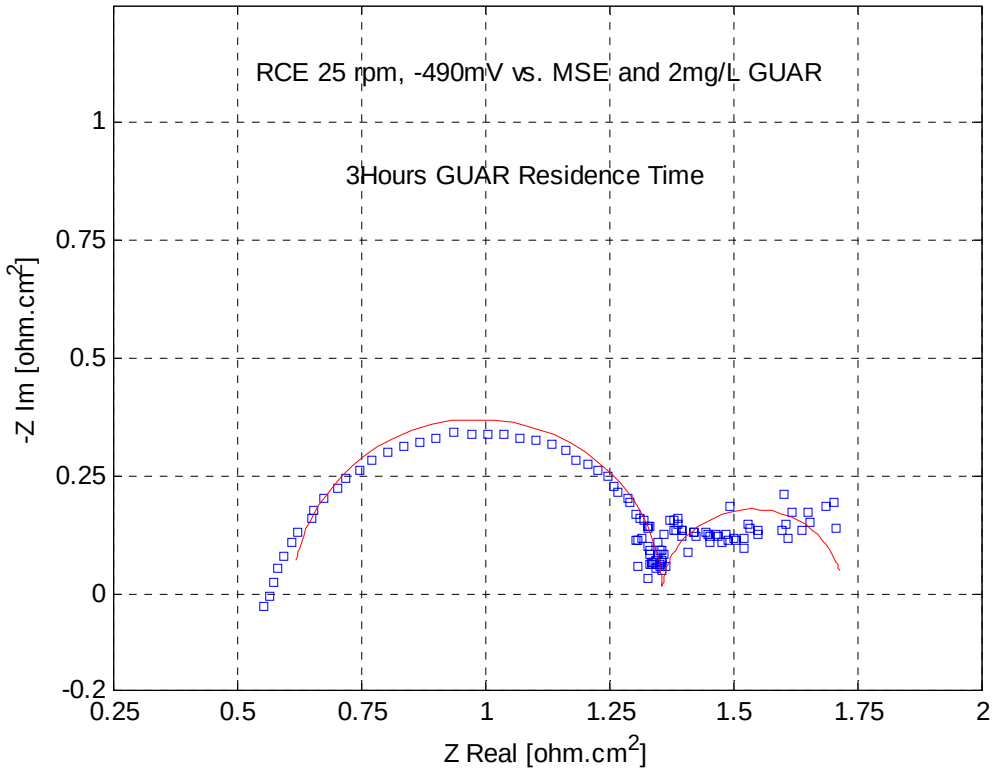

Figure 5: Complex-Plane Plot of Experimental and Simulated Impedance Spectra at 45°C in the Presence of Guar at -490mV vs. MSE and 3Hours Residence Time

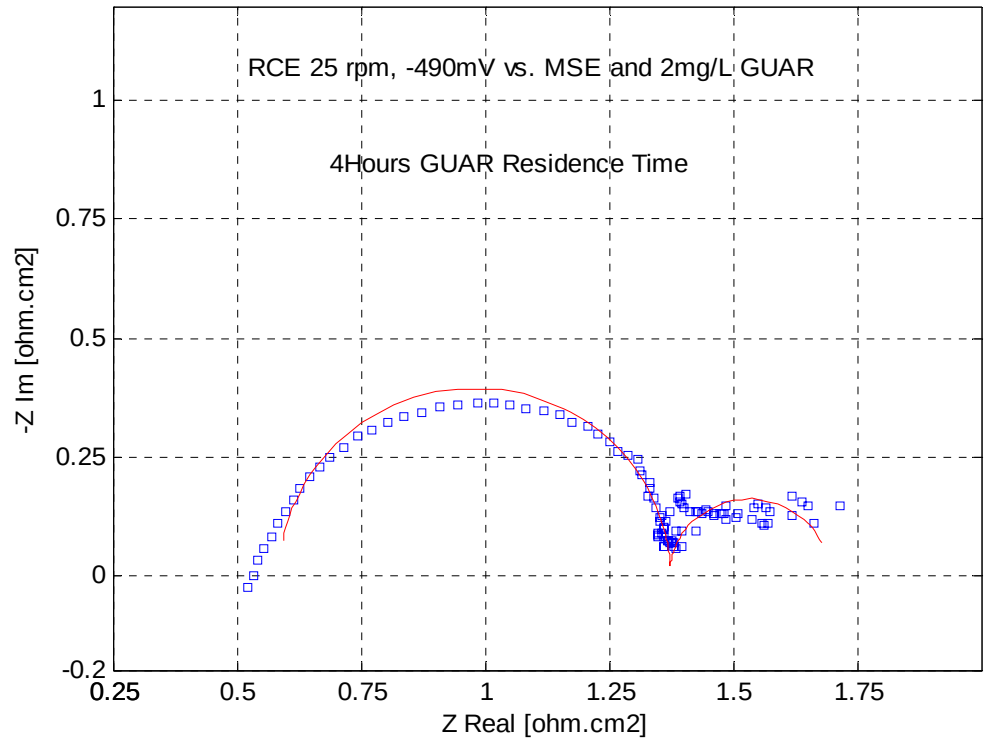

Figure 6: Complex-Plane Plot of Experimental and Simulated Impedance Spectra at 45°C in the Presence of Guar at -490mV vs. MSE and 4Hours Residence Time

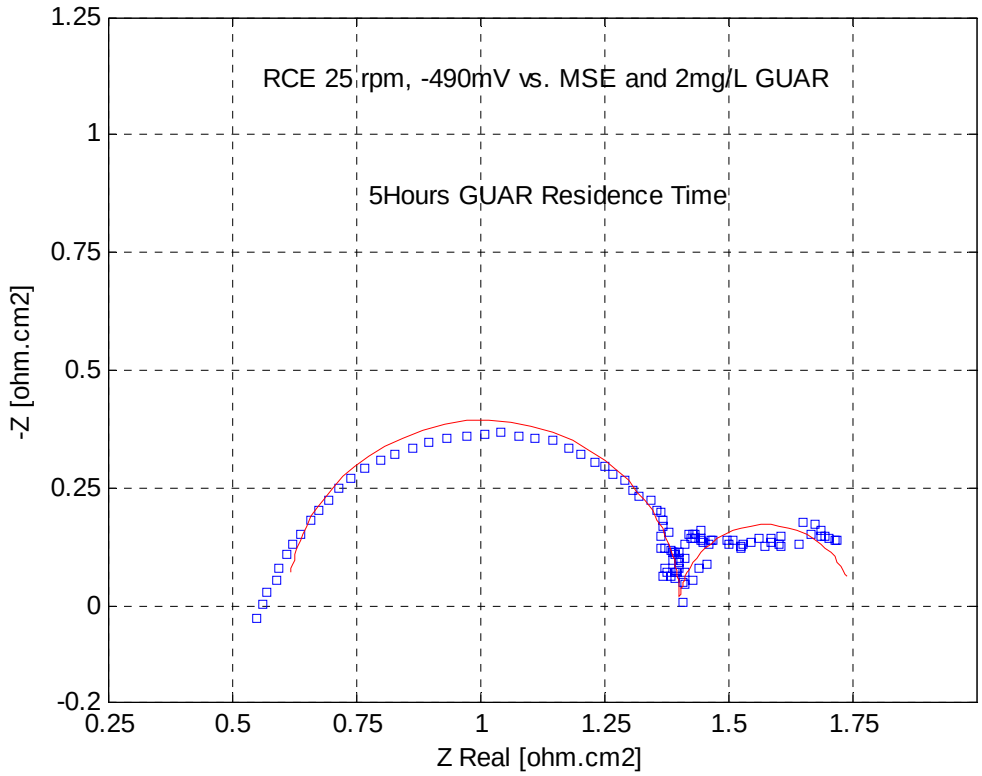

Figure 7: Complex-Plane Plot of Experimental and Simulated Impedance Spectra at 45^{o}C in the Presence of Guar at -490mV vs. MSE and 5Hours Residence Time

ELECTROCHEMICAL IMPEDANCE DATA USING APAM AT -470mV vs. MSE AND 45^{o}C

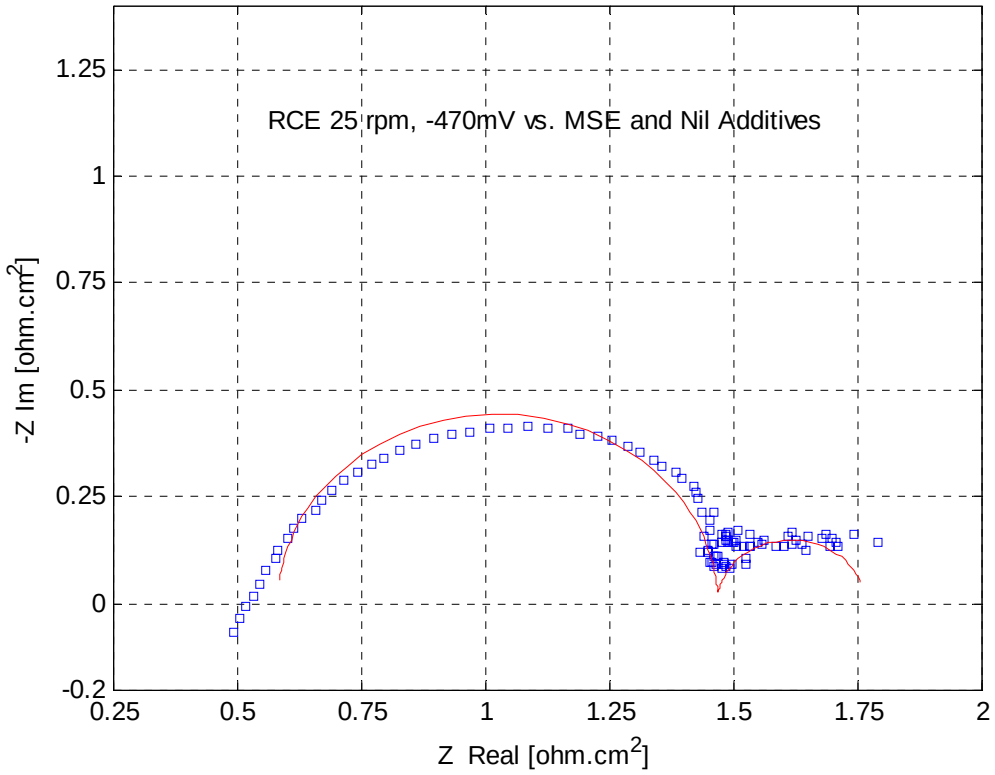

Figure 8: Complex-Plane Plot of Experimental and Simulated Impedance Spectra at 45°C in the Absence of APAM at -470mV vs. MSE

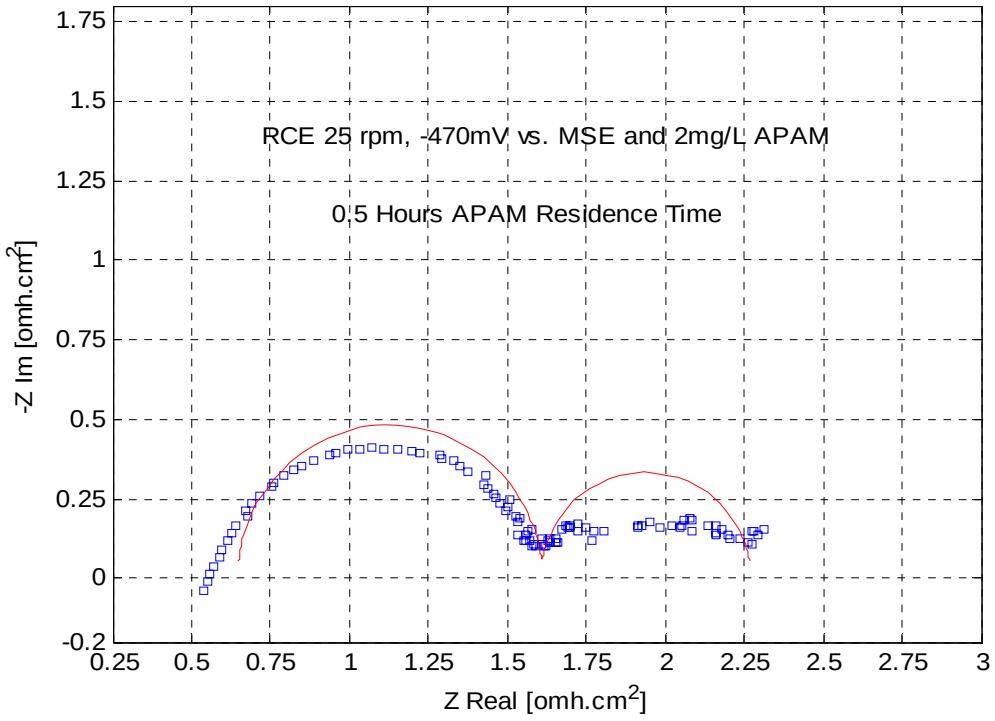

Figure 9: Complex-Plane Plot of Experimental and Simulated Impedance Spectra at 45°C in the Presence of APAM at -470mV vs. MSE and 0.5Hours Residence Time

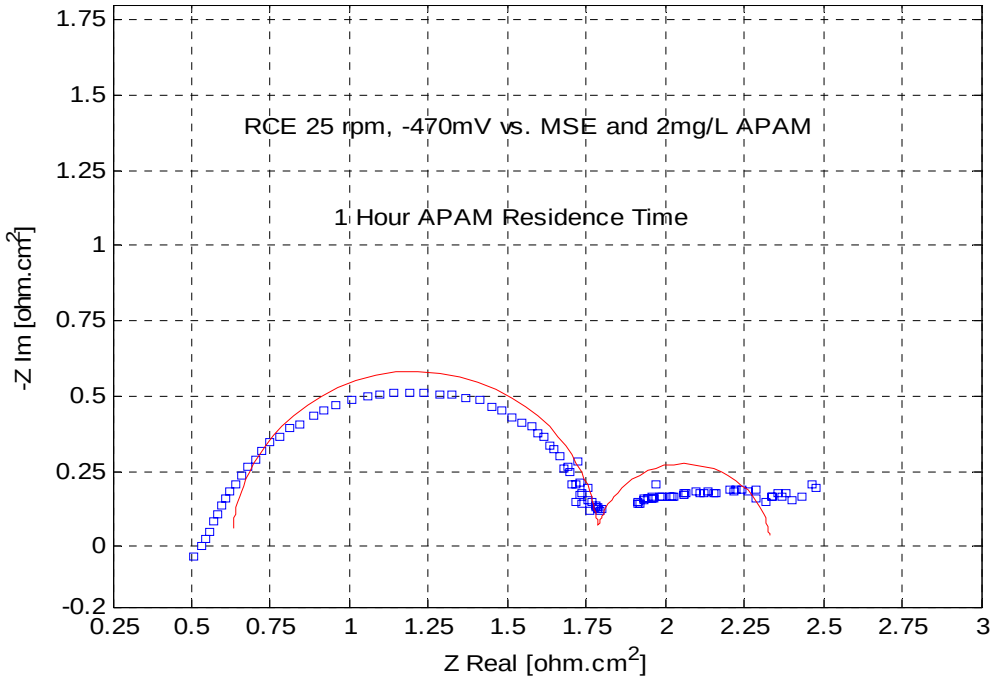

Figure 10: Complex-Plane Plot of Experimental and Simulated Impedance Spectra at 45°C in the Presence of APAM at -470mV vs. MSE and 1Hour Residence Time

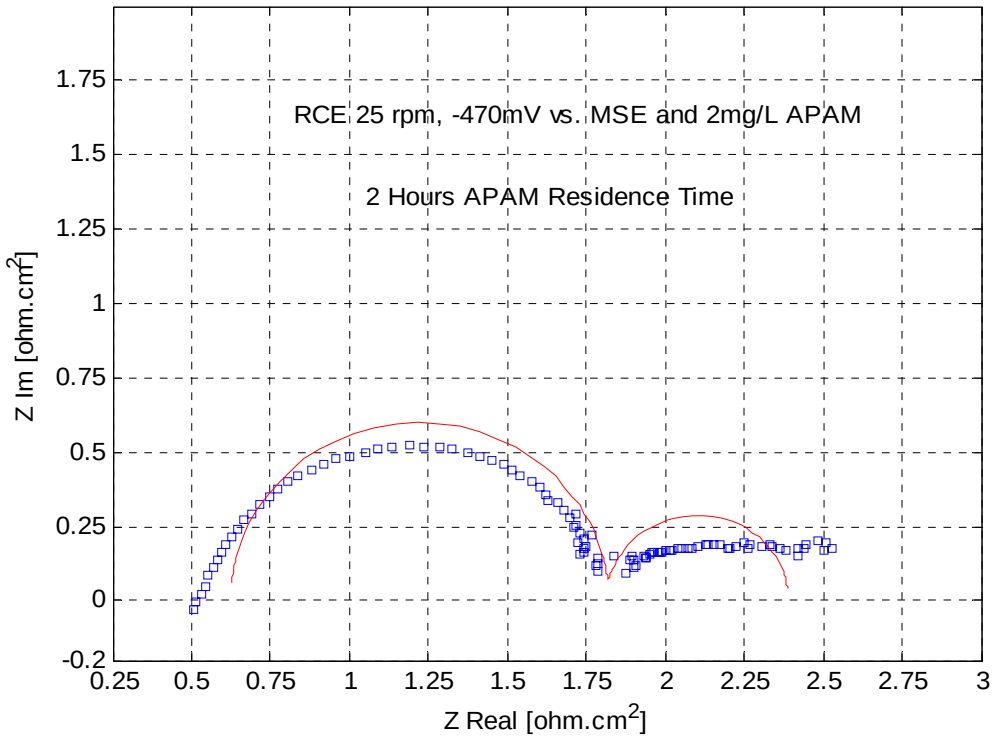

Figure 11: Complex-Plane Plot of Experimental and Simulated Impedance Spectra at 45°C in the Presence of APAM at -470mV vs. MSE and 2Hours Residence Time

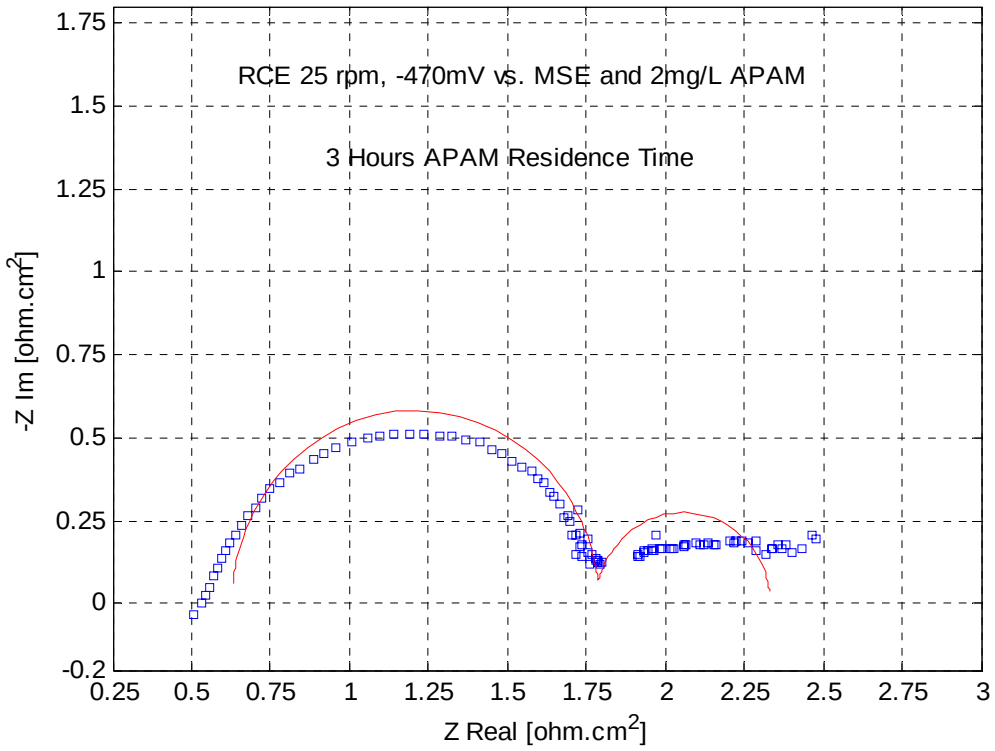

Figure 12: Complex-Plane Plot of Experimental and Simulated Impedance Spectra at 45°C in the Presence of APAM at -470mV vs. MSE and 3Hours Residence Time

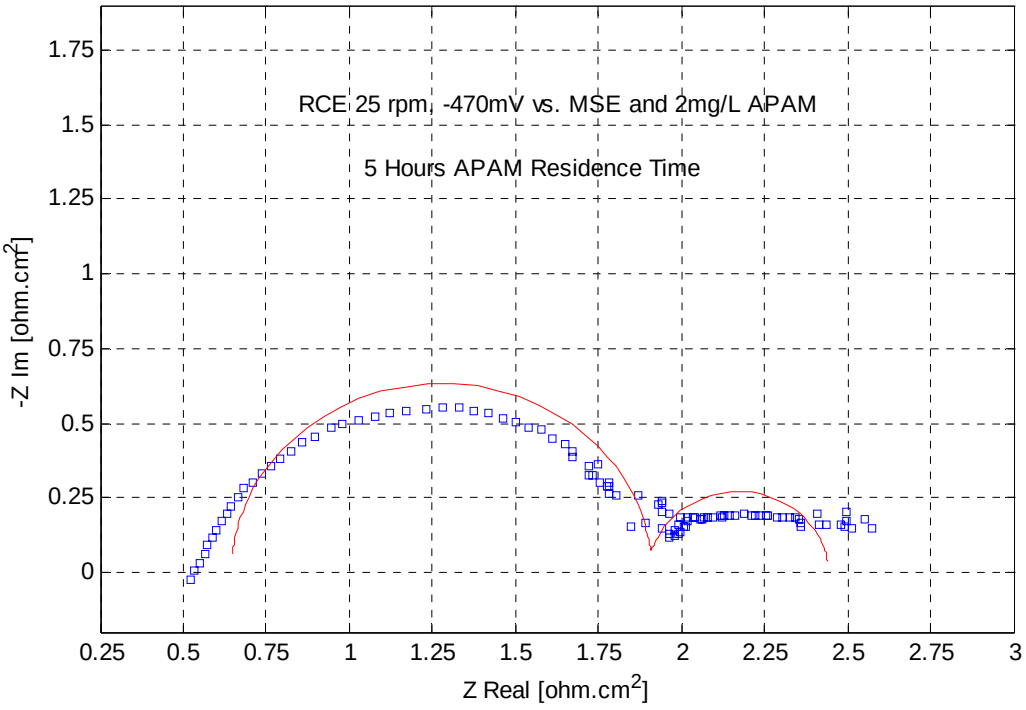

Figure 13: Complex-Plane Plot of Experimental and Simulated Impedance Spectra at 45°C in the Presence of APAM at -470mV vs. MSE and 5Hours Residence Time

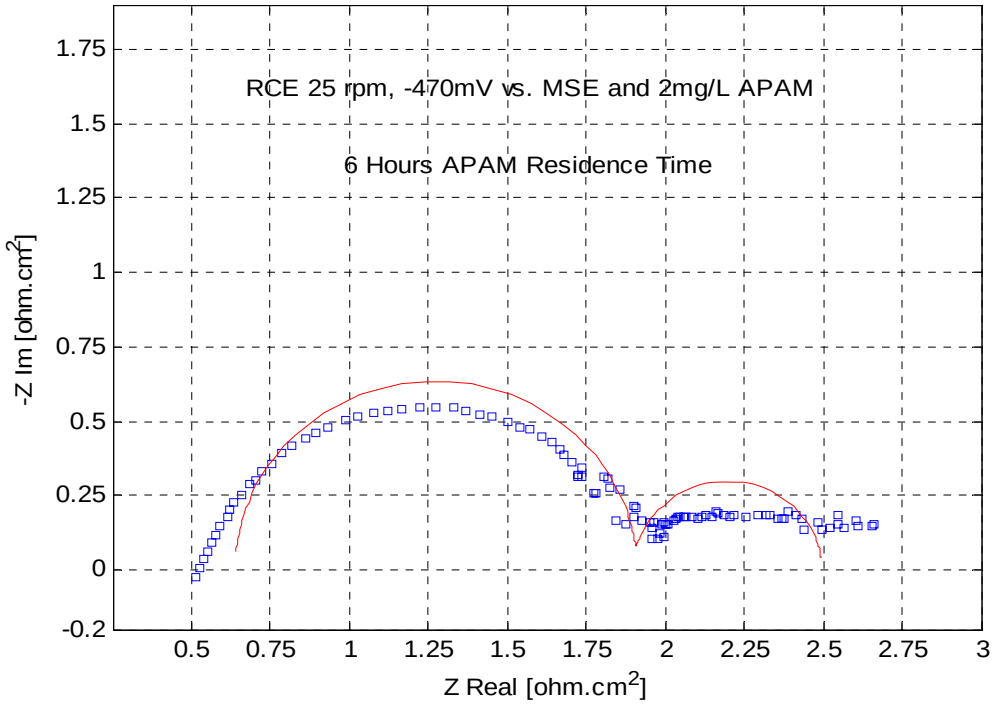

Figure 14: Complex-Plane Plot of Experimental and Simulated Impedance Spectra at 45°C in the Presence of APAM at -470mV vs. MSE and 6Hours Residence Time

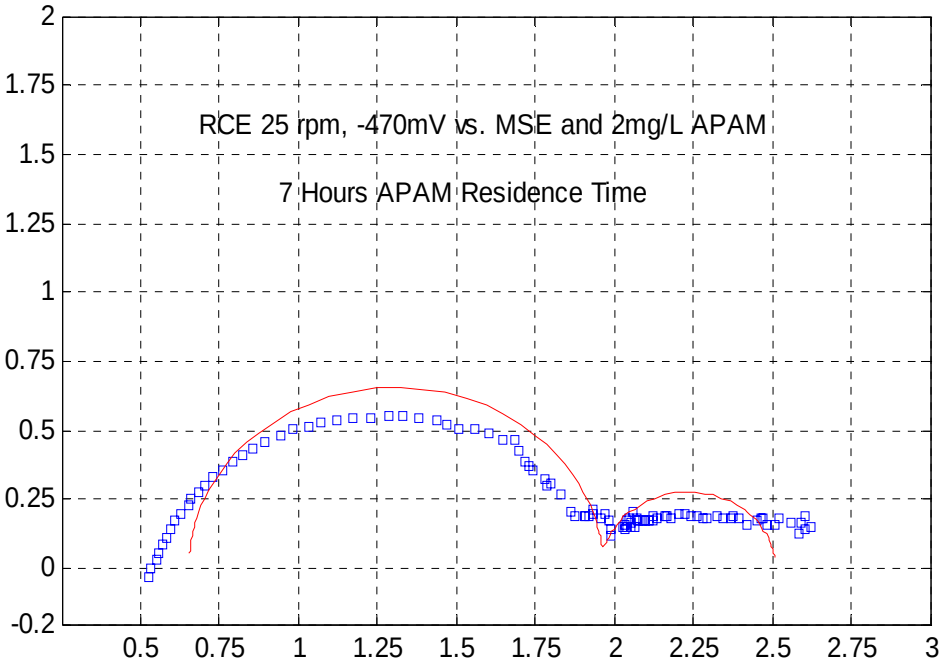

Figure 15: Complex-Plane Plot of Experimental and Simulated Impedance Spectra at 45°C in the Presence of APAM at -470mV vs. MSE and 7Hours Residence Time.

ELECTROCHEMICAL IMPEDANCE DATA USING APAM AT -490mV vs. MSE AND 45^{o}C

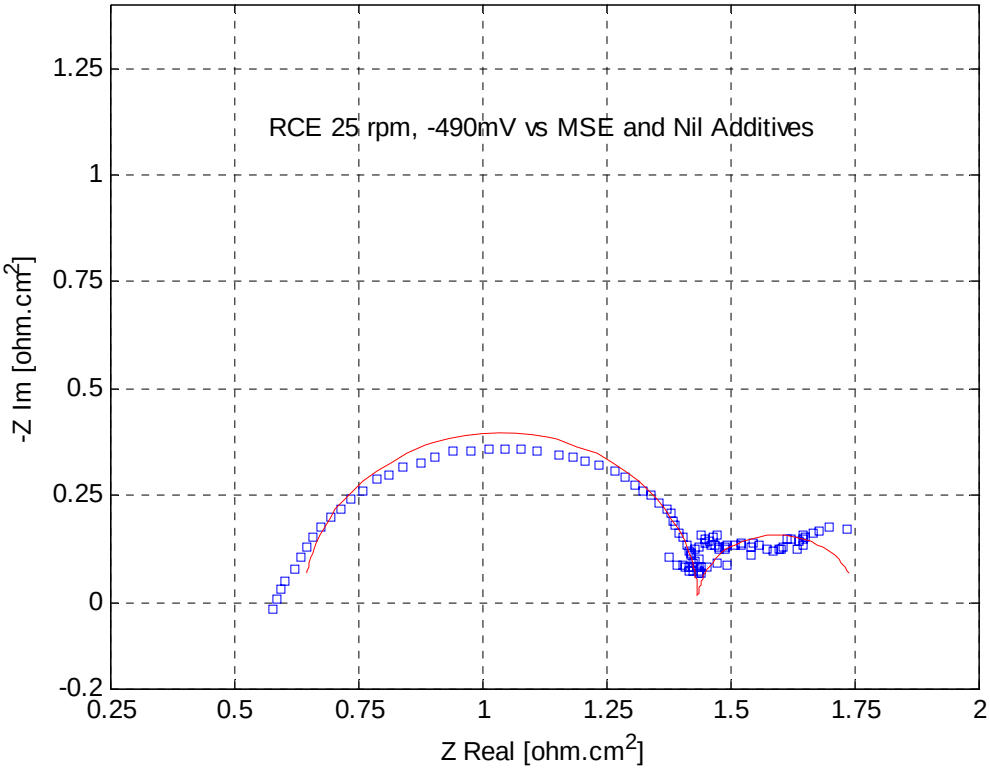

Figure 16: Complex-Plane Plot of Experimental and CNLS Simulated Impedance Spectra in the Absence of APAM at 45°C and -490mV versus MSE

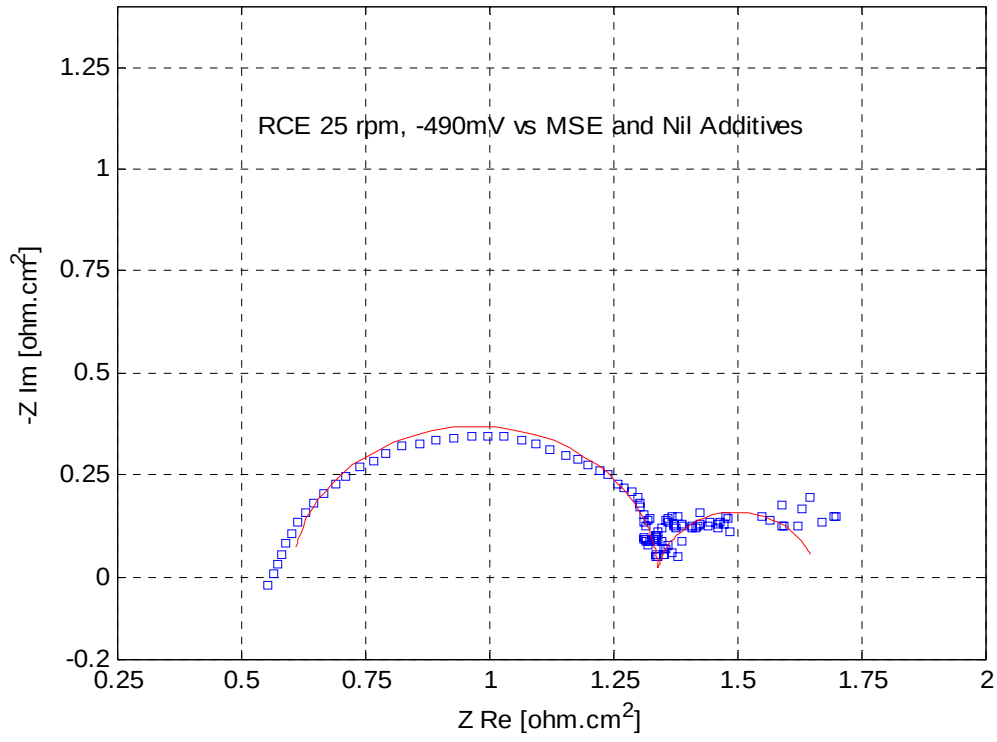

Figure 17: Complex-Plane Plot of Experimental and CNLS Simulated Impedance Spectra in the Absence of APAM at 45°C and -490mV versus MSE

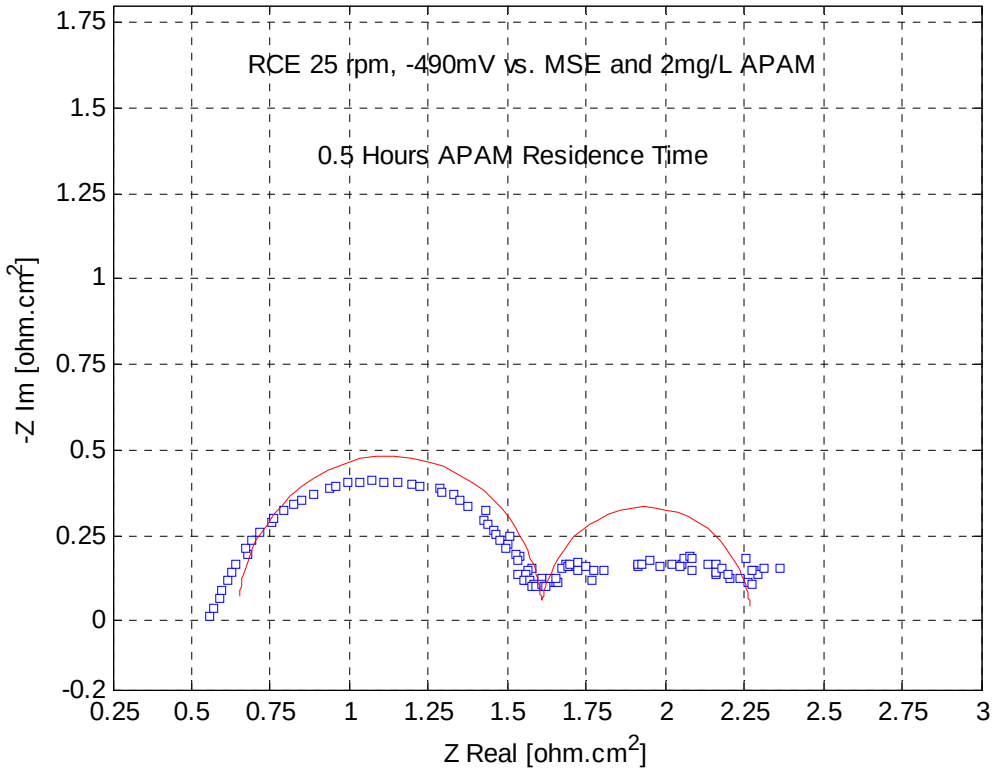

Figure 18: Complex-Plane Plot of Experimental and Simulated Impedance Spectra at 45°C in the Presence of APAM at -490mV vs. MSE and 0.5Hours Residence Time.

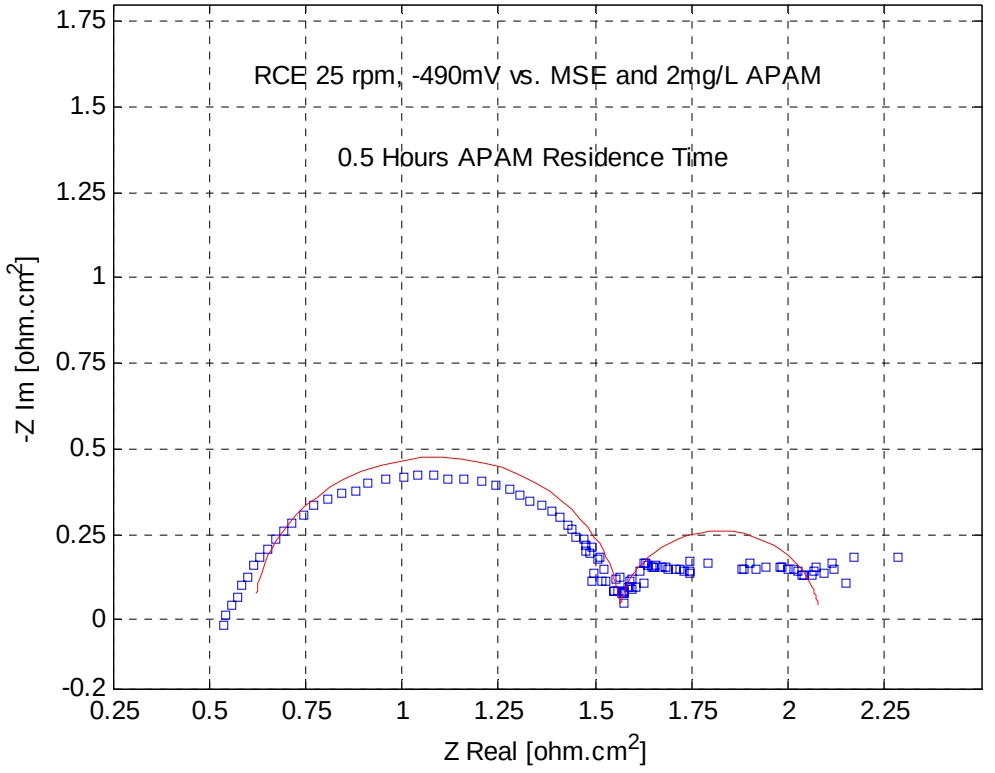

Figure 19: Complex-Plane Plot of Experimental and Simulated Impedance Spectra at 45°C in the Presence of APAM at -490mV vs. MSE and 0.5Hours Residence Time.

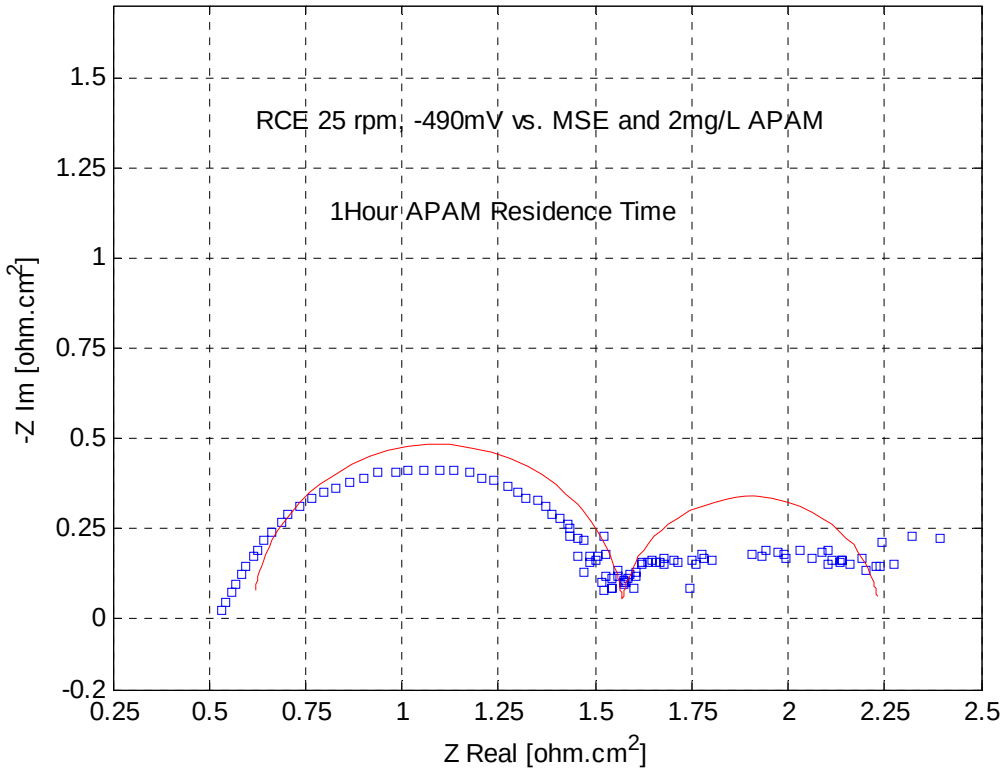

Figure 20: Complex-Plane Plot of Experimental and Simulated Impedance Spectra at 45°C in the Presence of APAM at -490mV vs. MSE and 1Hour Residence Time.

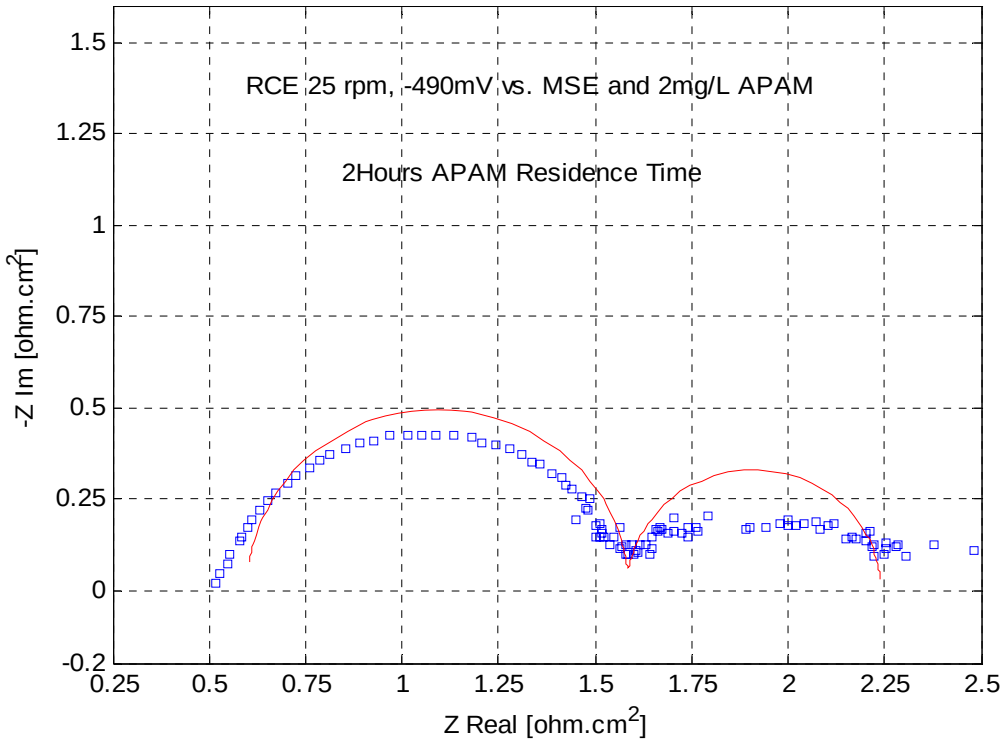

Figure 21: Complex-Plane Plot of Experimental and Simulated Impedance Spectra at 45°C in the Presence of APAM at -490mV vs. MSE and 2Hours Residence Time.

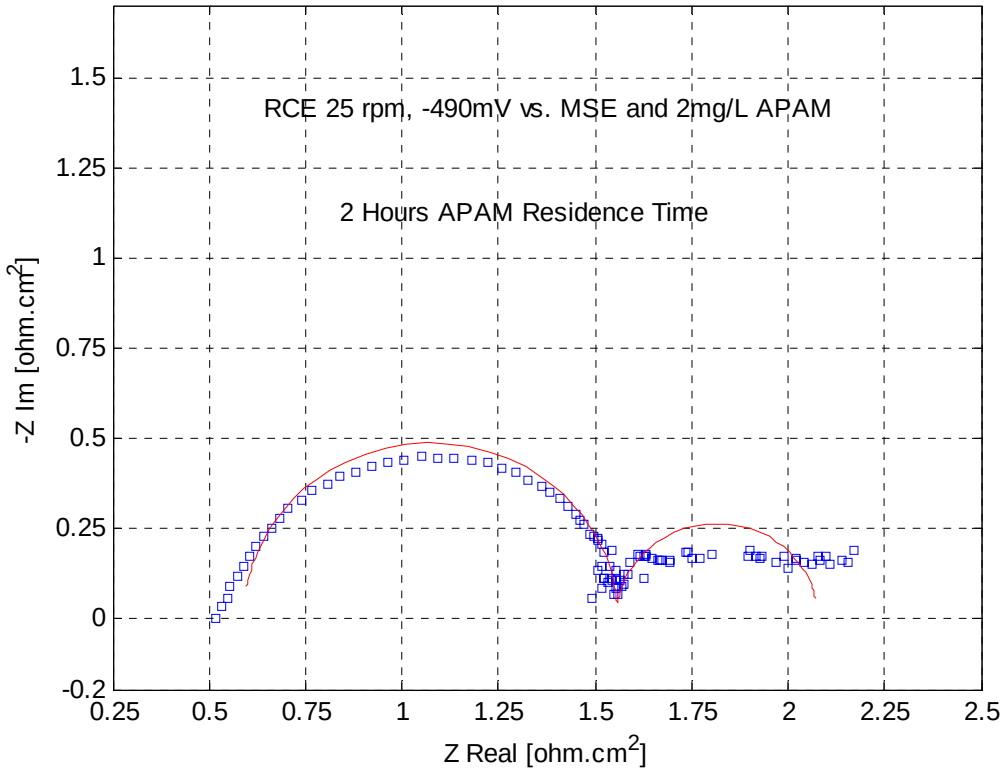

Figure 22: Complex-Plane Plot of Experimental and Simulated Impedance Spectra at 45°C in the Presence of APAM at -490mV vs. MSE and 2Hours Residence Time (T2)

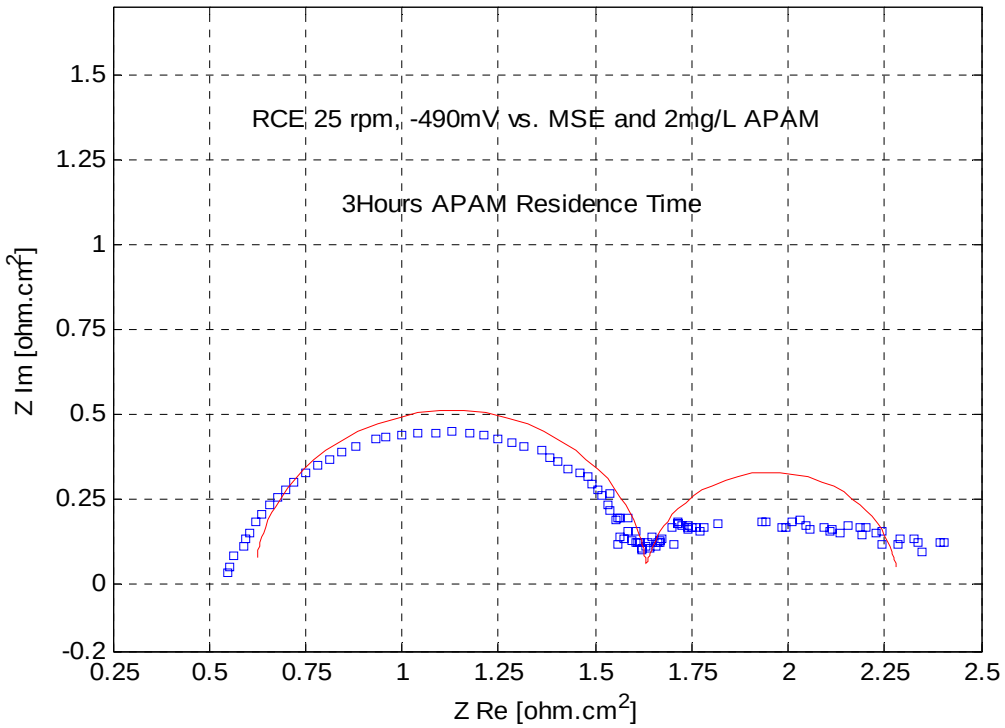

Figure 23: Complex-Plane Plot of Experimental and Simulated Impedance Spectra at 45°C in the Presence of APAM at -490mV vs. MSE and 3Hours Residence Time

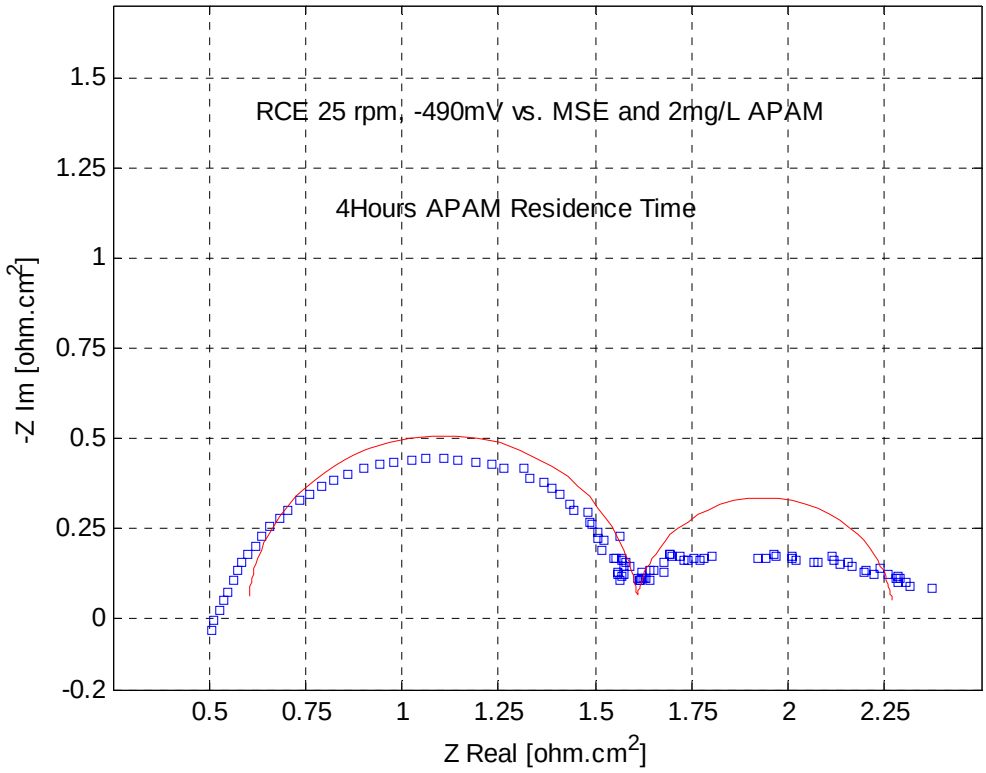

Figure 24: Complex-Plane Plot of Experimental and Simulated Impedance Spectra at 45°C in the Presence of APAM at -490mV vs. MSE and 4Hours Residence Time.

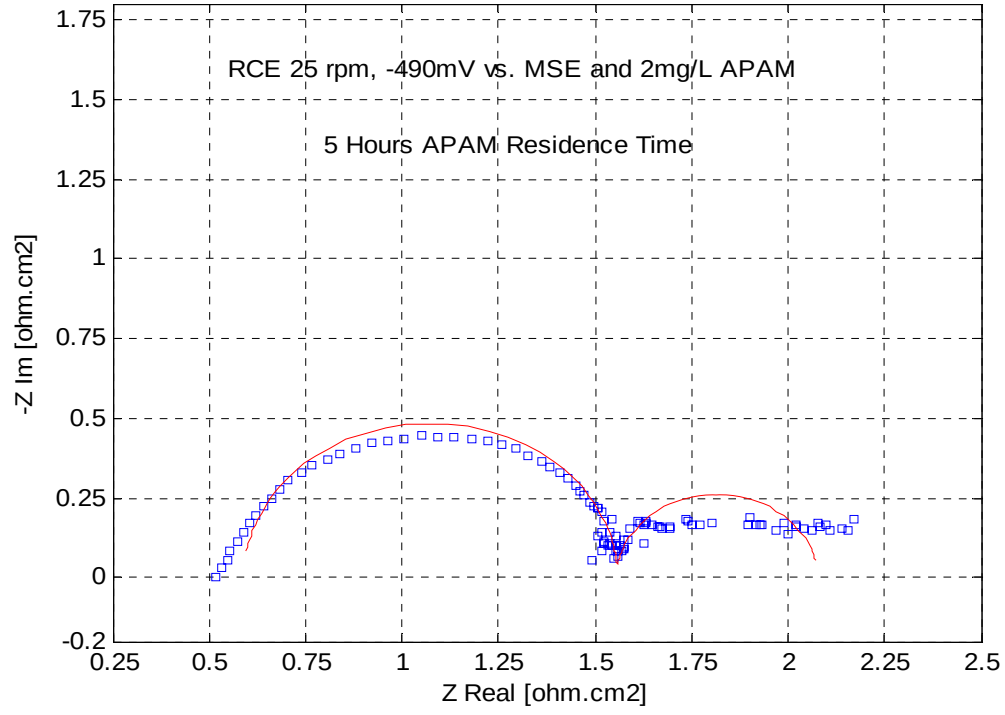

Figure 25: Complex-Plane Plot of Experimental and Simulated Impedance Spectra at 45°C in the Presence of APAM at -490mV vs. MSE and 5Hours Residence Time

ELECTROCHEMICAL IMPEDANCE DATA USING APAM AT -445mV vs. MSE AND 64^{o}C

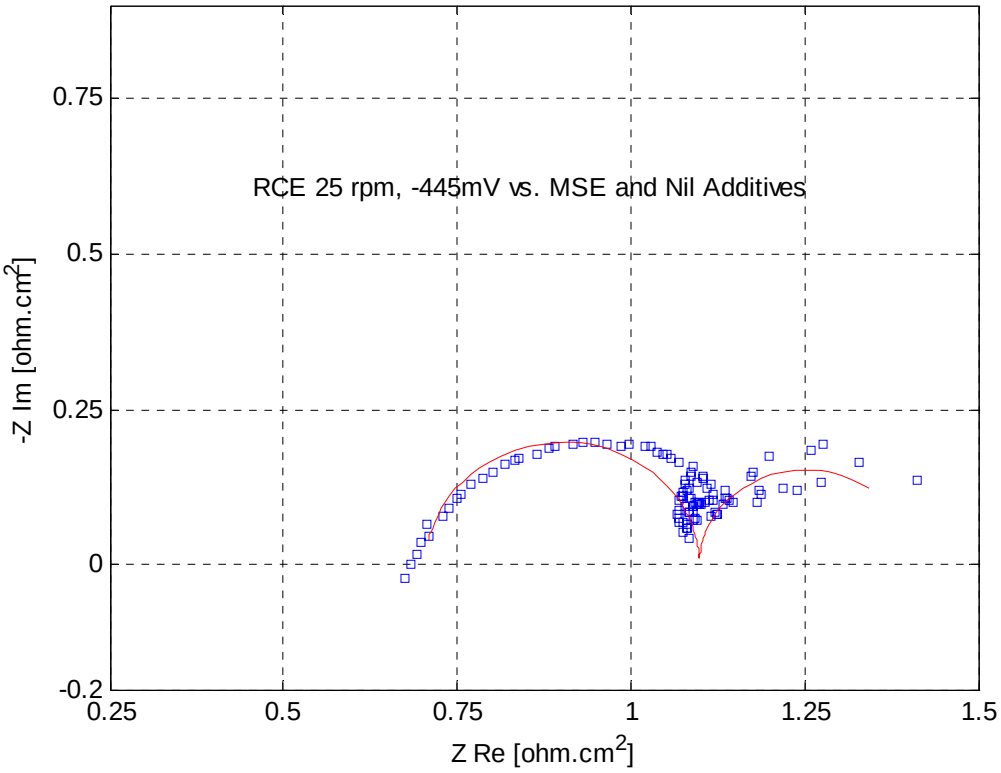

Figure 26: Complex-Plane Plot of Experimental and Simulated Impedance Spectra at 64°C in the Absence of APAM at -445mV vs. MSE

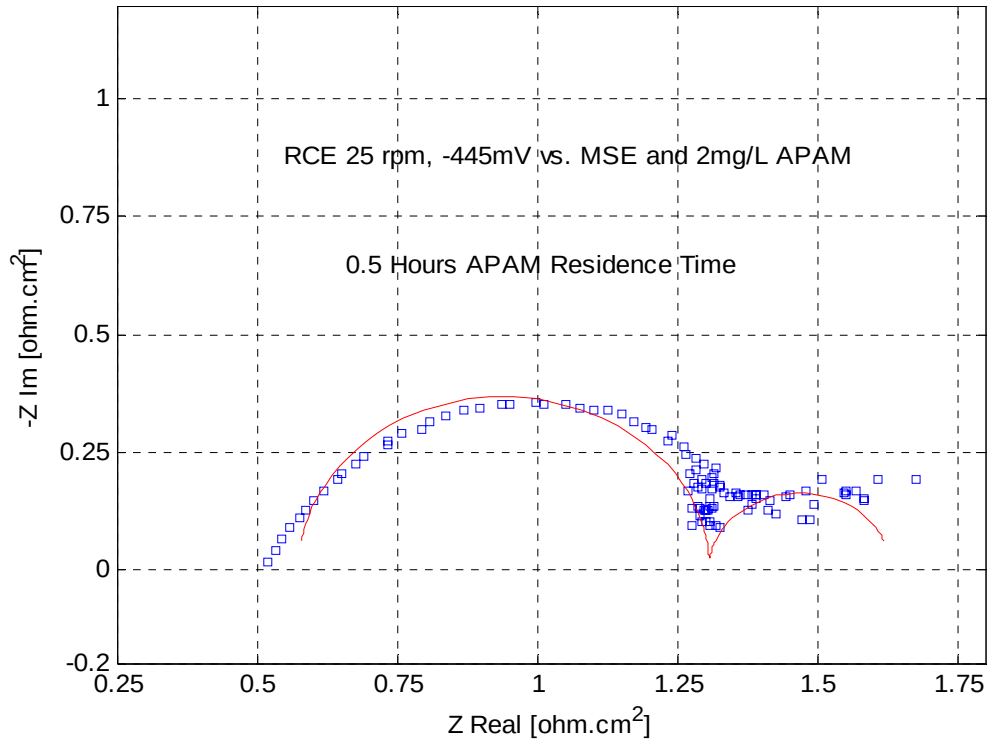

Figure 27: Complex-Plane Plot of Experimental and Simulated Impedance Spectra at 64°C in the Presence of APAM at -445mV vs. MSE and 0.5Hours Residence Time

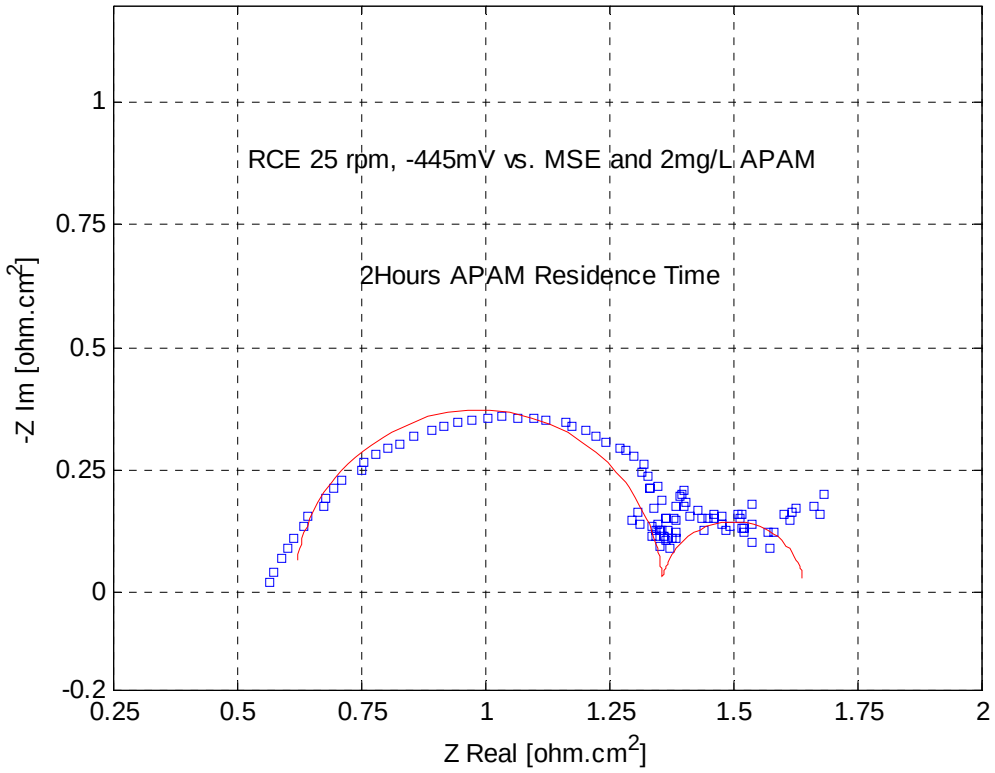

Figure 28: Complex-Plane Plot of Experimental and Simulated Impedance Spectra at 64°C in the Presence of APAM at -445mV vs. MSE and 2Hours Residence Time

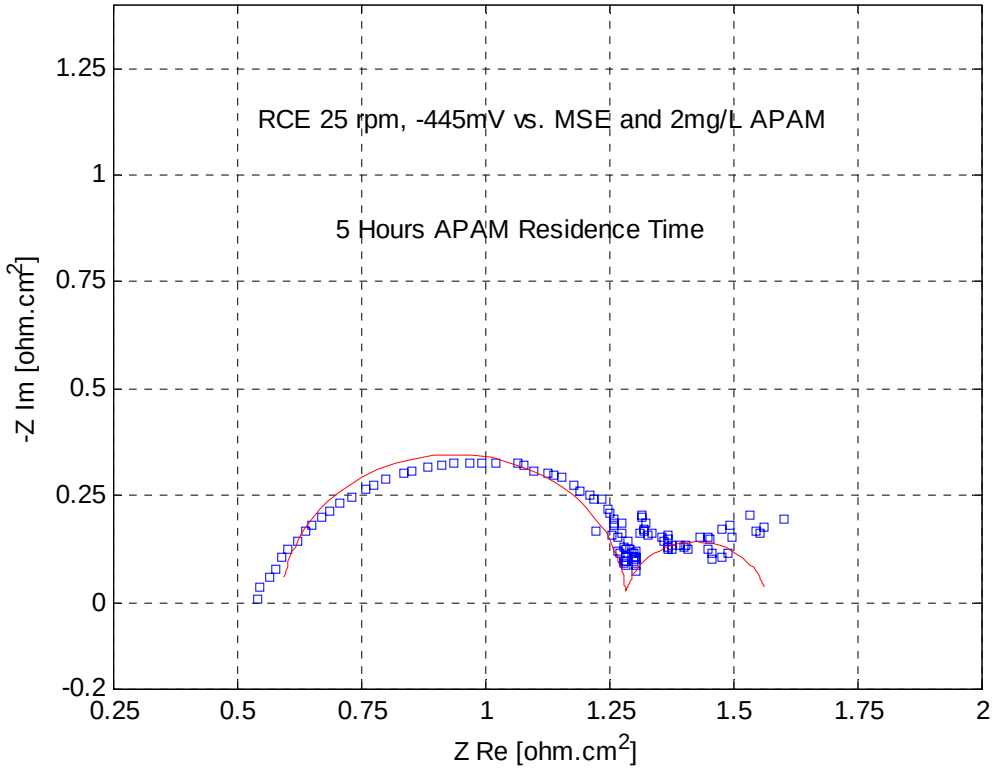

Figure 29: Complex-Plane Plot of Experimental and Simulated Impedance Spectra at 64°C in the Presence of APAM at -445mV vs. MSE and 5Hours Residence Time

ELECTROCHEMICAL IMPEDANCE DATA USING A ROTATING DISC ELECTRODE AT 25 RPM

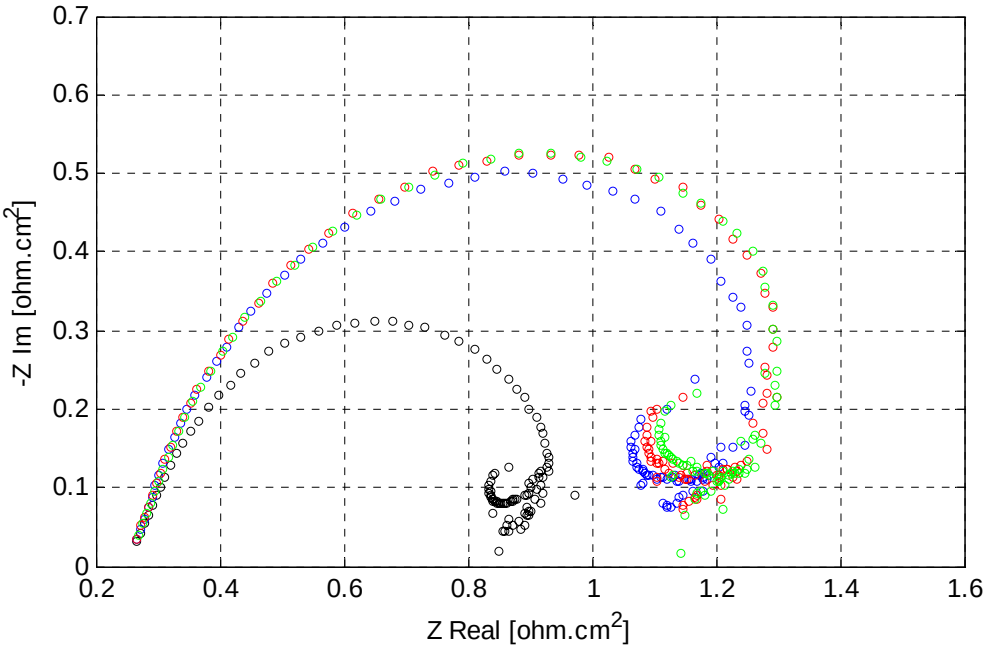

Figure 30: Complex-Plane Plot using RDE at 25 rpm and 45°C (50kHz-0.2Hz). Black – Control without APAM, Blue – 1 Hrs, Red – 3Hrs. and Green – 6Hrs.

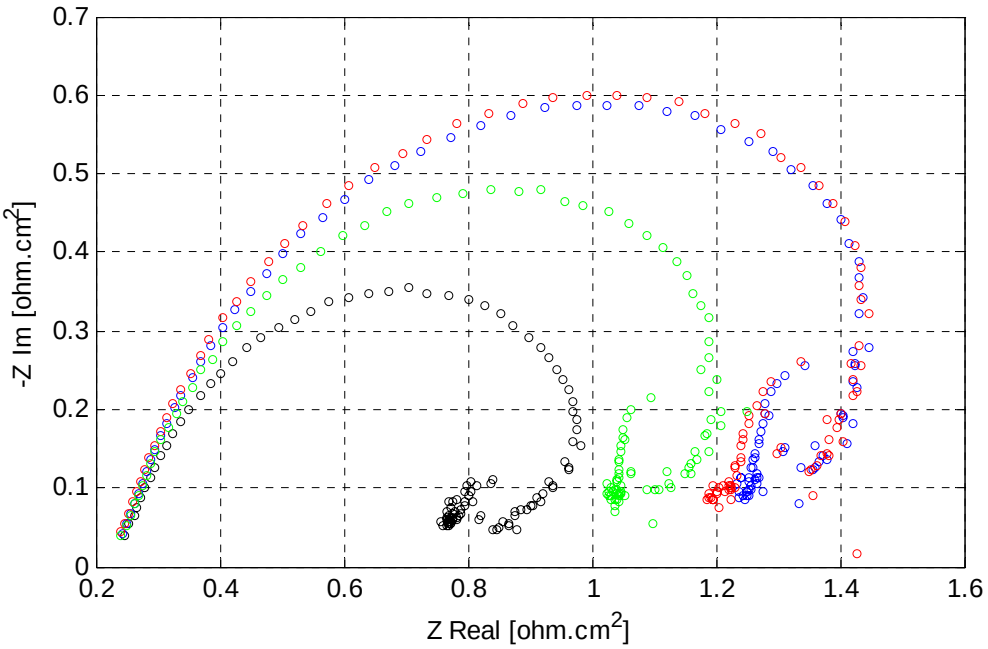

Figure 31: Complex-Plane Plot using RDE at 25 rpm and 64°C (50kHz-0.2Hz). Black – Control without APAM, Blue – 1 Hrs, Red – 3Hrs. and Green – 6Hrs.

<HYDROMETALLURGY 2003: 5th INTERNATIONAL SYMPOSIUM IN HONOR OF PROFESSOR IAN RITCHIE> *< Edited by C.A. Young, A.M. Alfantazi, C.G. Anderson, D.B. Dreisinger, B. Harris and A. James>*
TMS (The Minerals, Metals & Materials Society, <2003>

DETERMINATION OF CRYSTALLITE SIZE AND SURFACE ROUGHNESS OF COPPER DEPOSITS FOR ELECTROWINNING IN THE PRESENCE OF AN ORGANIC ADDITIVE

Cesimiro Fabian[a,b], Michael Ridd[b], Sharon Ness[c], Thomas Lancaster[d*] and Gregory Griffin[a]

[a]School of Engineering, James Cook University, Townsville, QLD., Australia
[b]School of Pharmacy and Molecular Sciences, James Cook University, Townsville, QLD., Australia,
[c]Advanced Analytical Center, James Cook University, Townsville, QLD., Australia,
[d*]Mount Gordon Operations, Western Metals Copper Limited, Gunpowder via Mount Isa, QLD., Australia,

Abstract

The crystallite size of copper electrodeposits was determined by X-Ray powder diffraction analysis using a General Area Detector Diffraction Solution (GADDS) diffractometer. Crystallite size was calculated for copper thin films which were deposited on a 316 stainless steel rotating cylinder electrode (RCE) in the presence and absence of additive "A". The crystallite size was calculated from a corrected full width at half maximum (FWHM) of the [110] peak profile using the Scherrer equation. The test of significant difference on crystallite size was derived using Kruskal-Wallis method. It was found that in the absence of the additive the median crystallite size was 426Å, which decreased to 364Å in the presence of the additive. As the additive degraded, the crystallite size increased to a size similar to that observed in the absence of additive.

1. Introduction

In the past 10 years, a lot of effort has been committed to understanding the role of additives in copper electrodeposition for the fabrication of interconnects in the microelectronics industry. However, relatively little has been published for copper deposition used in electrorefining and electrowinning. Both copper deposition in electrorefining and fabrication of interconnects requires dosing of organic additives into the electrolyte bath. The additives, commonly known as leveling agents, surfactants, grain refiners and brighteners produce smooth deposits by reducing dendrite growth or, in other terms, to promote superconformal growth for the fabrication of interconnects.

The role of the leveling agent is to reduce the charge transference at the entrances of the vias, protrusions or peaks and consequently to increase charge transference in the vias or valleys to attain smooth deposit or superconformal growth. The role of the grain refiner is to create new nucleates to form new crystallites that possibly enhance new microcurrent distribution.

---

*Present address: Straits Resources, WA, Australia

In this paper, we present a new technique (GADDS) to yield the mean crystallite dimensions of electrowon copper and limited information about their size distribution as well. This process control tool indicates that precision in terms of reproducibility is more important than absolute accuracy. This tool could be useful for quality-control comparisons to evaluate an additive system for the fabrication of interconnects, electrorefining and electrowinning.

The initial stages of 2D and 3D metal phase formation under electrochemical conditions are well understood on an atomic level and these nucleation processes depend on the nature and concentration of the leveling agent[(1)]. In metal deposition, nucleation is a very important process; the first step of metal deposition is the formation of nuclei of the depositing metal on a foreign substrate and on a substrate of the native metal. It is stated by Budevski[(1)] that the competition between nucleation and growth determines the smoothness of the deposit: the higher the nucleation rate; the finer the crystal grains (crystal size) . Conversely, the forms of the growing crystals determine the physical appearance and structure: for a higher growth rate of the crystal grains normal to the substrate, a more fibrous structure is obtained. A brightening effect can be achieved from large developed crystal faces parallel to the substrate. Therefore, the kinetics of nucleation and growth play a dominant role in determining the overall deposition kinetics, as well as the appearance, structure and properties of the deposit.

A randomly-oriented dispersion (RD) type corresponds to an increased inhibition of the crystallization process by increasing the cathodic overvoltage. The additive system for the

fabrication of interconnects often referred to in the literature[2, 3] consists of polyethylene glycol (PEG) of 3350 molecular weight, Janus Green B (JGB), bis (3-sulfopropyl) disulfide (SPS) and chloride ions in 24 g/L copper and 180 g/L sulfuric acid at room temperature. The other additive system also often referred to consists of PEG, thiol (3-mercapto-1-propanesulfonate, MPSA) and chloride ions[2, 3]. It was reported that PEG, MPSA and chloride ions were required to produce a clear hysteresis from cycle voltammographs from which a superconformal growth was also achieved. In comparison, the leveling agent used throughout the *electrorefining* industry is animal (protein) glue; the grain refiner is thiourea and chloride ions in 40-50 g/L copper and 150-180 g/L sulfuric acid at 62°C. Glue is a long-chain amino acid compound undergoing constant degradation by which the long-chain becomes shortened and protonated. The additions of fresh glue, thiourea and chloride ions are closely monitored in electrorefining plants and the dosing ratio of thiourea/glue are kept almost constant at about two.

The mechanism of the leveling effect of glue is thought to be due to the protonated ends of the glue becoming attached predominantly to the protrusions or peaks of the copper cathode. Therefore the mass transference of copper is minimized on these protrusions producing a rounded/smoothed deposit. The grain refiner, thiourea, also undergoes constant degradation, forming complexes with cuprous and cupric ions and its role is to create new nuclei on the deposit to possibly facilitate the growth of new crystals. In contrast, copper deposition in *electrowinning* uses only guarfloc (guar), a polysaccharide, and chloride ions as the additive system. It is known[4] that polysaccharides act as brighteners and that guar is a weaker leveling agent or weaker polarizer than animal glue.

In this paper we report the results of a study that investigates the use of a recently developed X-ray diffraction (XRD) spectrometer, General Area Detector Diffraction Solution (GADDS) diffractometer which allows for the collection of a large number of XRD spectra from electrowon copper sample over a small area. Using GADDS, it is possible to measure the effect of organic additives on crystallite sizes of electrowon copper and to assess the efficacy of the organic additive.

1.1 Line Broadening Principles for Crystallite Size

It is widely known that copper deposits as face centered cubic (fcc) crystals and a crystallite is the smallest diffracting domain in a material. It is important to note that the crystallite size is therefore different from, but maybe related to, particle size measured, for example with an electron microscopy.

In the absence of lattice of lattice strains or other imperfections in significant amounts, the breadth β of the pure diffraction profile can be used to calculate the crystallite size of a sample[5, 6]. The Sherrer equation (4) can be used to estimate the mean crystallite dimensions.

$$L = \frac{K.\lambda}{\beta.\cos\theta} \qquad \textbf{[1]}$$

where θ and λ are the Bragg angle and x-ray diffraction wavelength in angstroms (Å), respectively. β is the line breath, commonly known as the full width at half maximum (FWHM) intensity of the peak in radians corrected for instrumental broadening using a Gaussian profile fit ($\beta^2 = U^2 – S^2$; U = copper sample, S = standard)[5]. K, λ and θ are 0.9, 1.54184 and 15 degrees, respectively.

The Scherrer equation shows an inverse relationship between crystallite size and peak profile width: the wider the peak, the smaller the crystallites and a particle may be comprised of many crystallites.

1.2 Derivation of Diffusion Layer Thickness

A program was developed using Mathcad2001i[7] to derive the diffusion layer thickness for the RCE. The physicochemical properties of the electrolyte was obtained from the data of Price and Davenport[8, 9]. The equation for the rotating cylinder electrode is formulated as[10, 11]:

$$i_L = 0.079 \frac{nFDC_b}{d} \mathrm{Re}^{0.7}\, Sc^{0.356} \qquad [2]$$

where i_L is the limiting current density; d is the diameter of the inner cylinder, the rotating cylinder; Re, the Reynolds number ($d^2*\omega/\nu$) and Sc the Schmidt number (ν/D). n is the number of electrons transferred in the electrode reaction; F, Faraday's constant; D, diffusion coefficient of electrolyte, cm^2/s and C_b copper concentration, mol/cm^3. Finally, the Nernst diffusion model was applied to calculate the diffusion layer thickness[12].

2. Experimental

A rotating cylinder electrode (RCE) was constructed in-house similar to the test unit described by Barkey, Muller and Tobias[11] and the electrowinning tests were conducted using this rotating cylinder electrode made of 316L stainless steel as cathode and a dimensionally stable anode (DSA) sourced from ELTECH Systems Corporation, USA. The active area of the RCE was $28cm^2$ and 12,000 coulombs were applied to each test. The electrode gap was 40mm and the RPM of the RCE was controlled using a Movitrac controller and 0.37kW motor (RF27D17104) with gear box both from SEW Eurodrive.

The initial concentrations of the components of the electrolyte were: copper, 36 g/L; sulfuric acid, 160 g/L and chloride ions, 25 mg/L and the initial electrolyte volume was 3.75L. Additive "A" was dissolved in 16-fold diluted synthetic electrolyte for two hours at 50°C to promote its degradation, unless otherwise stated. Additive "A" was dosed to the electrolyte at 1mg/L, and thoroughly mixed in the electrolyte for approximately 20 minutes before a potential was applied to the EW cell.

The surface roughness of the deposit copper was measured using a Mahr Perthometer M1 using a 2μm stylus tip and calibrated with its PGN-3 (Rz = 2.9 μm) standard. The surface roughness measurement was conducted before the copper deposit was detached from the RCE at 8 equidistantly distributed areas along the height of the electrode.

X-Ray diffraction data was collected using a Siemens/Bruker General Area Detector Diffraction Solution, GADDS diffractometer at the Advanced Analytical Center of James Cook University. The instrumental parameters such as collimator size, detector resolution and beam divergence critically affect line broadening for the determination of peak broadening. Table 1 summarizes the instrumental parameters used to determine the peak broadening.

The GADDS diffractometer was set up to automatically map out 2cm^2 surface area from the 28 cm^2 copper deposits obtained from the electrowinning tests. It read in steps of 0.5mm until the full length of the Y-axis is completed and then it moved 0.5mm in the X-axis to read another full length of the Y-axis and successively to produce about 1450 readings per sample unless otherwise stated. Therefore, surface heterogeneity can be detected from the small and representative surface area to be analyzed from its XRD pattern.

Table 1: GADDS Diffractometer Parameters

Radiation	Cu
Sample-detector distance	30 cm
Collimator	500μm
kV, mA	40, 52
Data collection time/reading	60 sec
2θ, ω	70, 30
Step size, mm	0.5
Copper plate mapped area, cm^2	~2

2.1 Correction for Instrumental Line Broadening

Lanthanum hexaboride powder (LaB_6, 660a), line position and line shape standard, from the National Institute of Standards and Technology (NIST) was selected as the standard reference material (SRM). The NIST certificate states that the *Fundamental Parameters Approach* analysis for homogeneity testing and also for refinement of the FWHM using a Lorentzian profile indicated that LaB_6 displayed no strain broadening and the domain size was 2.0μm. Under the conditions stated above, the FWHM obtained for the LaB_6 SRM was 0.274 degrees, a value used to correct the FWHM of copper sample data for the effect of instrumental line broadening.

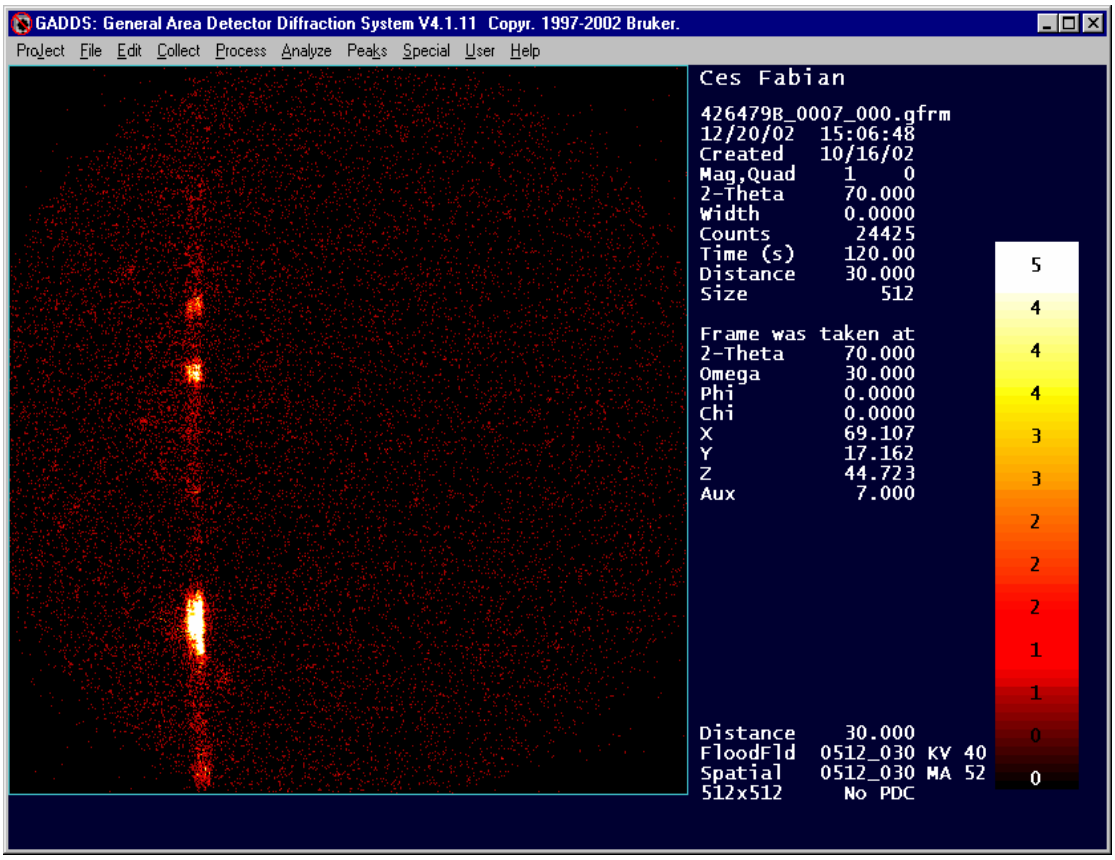

Figure 1: Typical frame from GADDS

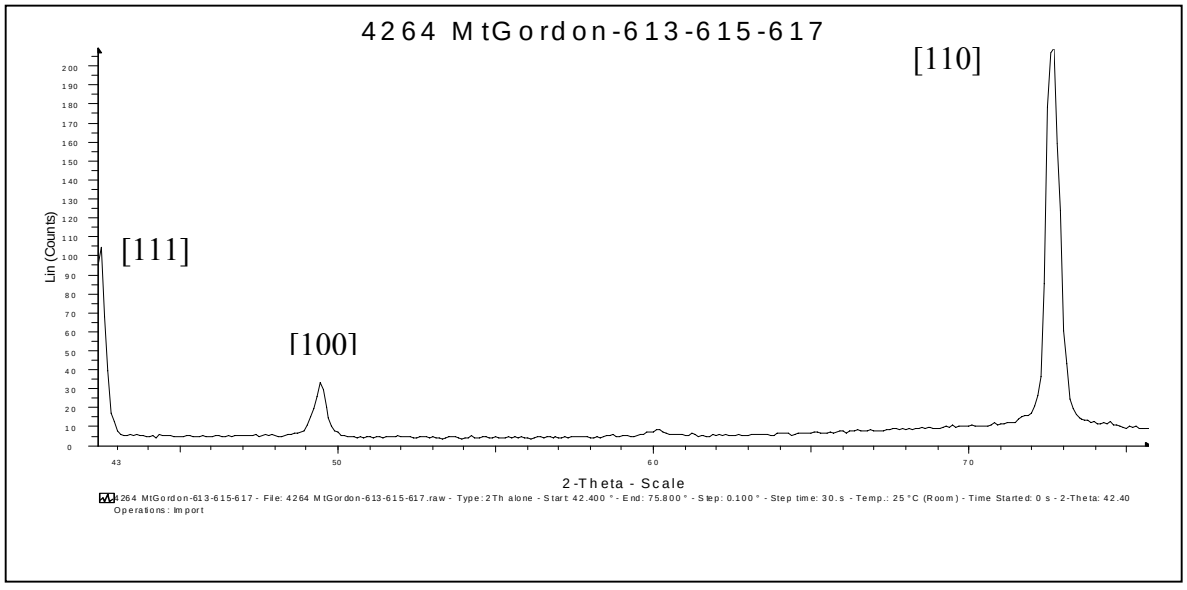

Figure 2: Typical preferred orientation profile: [110] >> [111] > [100]

The large spots in Figure 1 represent large crystallite sizes. The preferred orientation throughout this testwork was [110]>>[111]>[100] as observed in Figure 2. Ilgar and O'Keefe[13] has observed a similar orientation pattern in the presence of 20 mg/L chloride ions. Therefore the full width at half maximum was determined from the highest peak, i.e., the most common crystal orientation, the [110] preferred orientation.

The Full Width at Half Maximum (FWHM) was calculated from each profile using the EVA software from Bruker AXS.

3. Experimental Results

Table 2 shows the electrowinning conditions and surface roughness values obtained in the presence and absence of additive "A". It is noted that Tests 2 and 4 were conducted with the same electrolyte (3.75 L) and consequently, the small variations in concentration of both cupric and sulfuric acid insignificantly affected the deposition process.

Table 2: Electrowinning Conditions and Surface Roughness

Test No.	1	2	3	4
Additive "Ä" Qualitative Description	Nil	fresh	degraded	old
Additive "A" preparation, hrs		2	2	2
Additive "A" in electrolyte, hrs.		0-4	8-12	18-22
RCE rpm	10	10	10	10
EW time, hrs	4	4	4	4
Electrolyte temperature, ^{o}C	50	50	50	50
Current density, mA/cm^2	30	30	30	30
Surface roughness, Ra, µm	5.51±0.41	4.92±0.25	5.50±0.66	4.94±0.39

It is noted that the surface roughness in the absence of additive "A" at 10 RPM, equivalent to a 234 µm diffusion layer thickness and at 50^{o}C was 5.51 ± 0.41 µm. This value concurs with the range of values presented by Ilgar and O'Keefe[13] who studied the effect of 20 mg/L chloride ions on surface roughness in copper electrowinning and reported for 175 and 65 µm diffusion layer thicknesses with unstirred and stirred solutions, respectively. The values reported for unstirred solutions vary from 6.4 to 12.5 ± 0.50 µm at 30 and 40^{o}C, 25 and 35 mA/cm^2 and 6000 coulombs. The surface roughness for 65 µm diffusion layer thickness was reported to be 3.9 ± 0.50 µm. It is noted that although the copper and sulfuric acid concentrations were 36g/L and 160 g/L, respectively in the Ilgar and O'Keefe[13] study and this work, the concentration of chloride ions was 25 mg/L in this study and the electrowinning cell type was different in both studies. Therefore, the hydrodynamic equations to derive the diffusion layer thickness were also different.

In the presence of additive "A", the surface roughness from the present work appeared to be slightly lower than 5.51 ± 0.41 µm. It is noted that Tests 2 and 4 were conducted with the same electrolyte bath and it can be seen that the surface roughness for these tests slightly increases including their standard deviations.

Table 3 presents a summary of the results of the analysis of the GADDS data for each of the four electrowinning experiments. The FWHM data was analyzed using the Kruskal-Wallis nonparametric method to test significance of the difference between multiple groups using SPSS version 11.5 (2002 version). The Kruskal-Wallis test is a one-way analysis of variance by ranks; in contrast to ANOVA, it assumes nothing about the distribution of the test variable and it can be used to test ordinal variables. It tests the null hypothesis that multiple independent samples come from the same population.

As the crystallites above 4500Å in size could not be quantified due to instrument and standard limitations, the percentage of this unprocessed FWHM data is also presented in Table 3.

Table 3: Kruskal-Wallis Test Results for Crystallite Size Data

Test No.	1	2	3	4
FWHM No. Readings, N	1428	156	1479	1493
Crystallite Size No. Processed, N	1040	133	913	1102
Crystallites percentage > 4500 Å, %	27	15	38	26
Crystallite Size Mean Rank	1657	1333	1414	1716
Asymptotic. Sig., Monte Carlo Sig., 99% CI, lower and upper bounds	p = .0000			
Median Crystallite Size, Å	426	364	398	438

The Kruskal-Wallis test results indicate that the mean crystallite size differs between the four tests at the 99% confidence level. Thus it can be concluded that at least one of the four samples differs from the others. Inspection of Table 3 shows that the crystallite size mean rank and the median crystallite size decreased in the presence of additive "A' except for experiment 4 when the additive had undergone degradation at 50^{o}C for 18-22 hours and had become inactive.

It can be seen from Table 3 that the proportion of crystallites larger than 4500Å varied between the tests. When additive 'A' was degraded slightly smaller crystallites but distinctly more crystallites greater than 4500 Å were formed compared with nil additive, fresh additive and old additive. The data for Test 3 are consistent with the formation with the formation of relatively large proportion of small crystallites formed on top of large crystals.

Figure 3 shows the FWHM histograms and indicates that Test 3 has two distinct frequencies. The frequency conformed by FWHM values less than 0.274 degrees 2θ possibly represent crystallites greater than 4500Å.

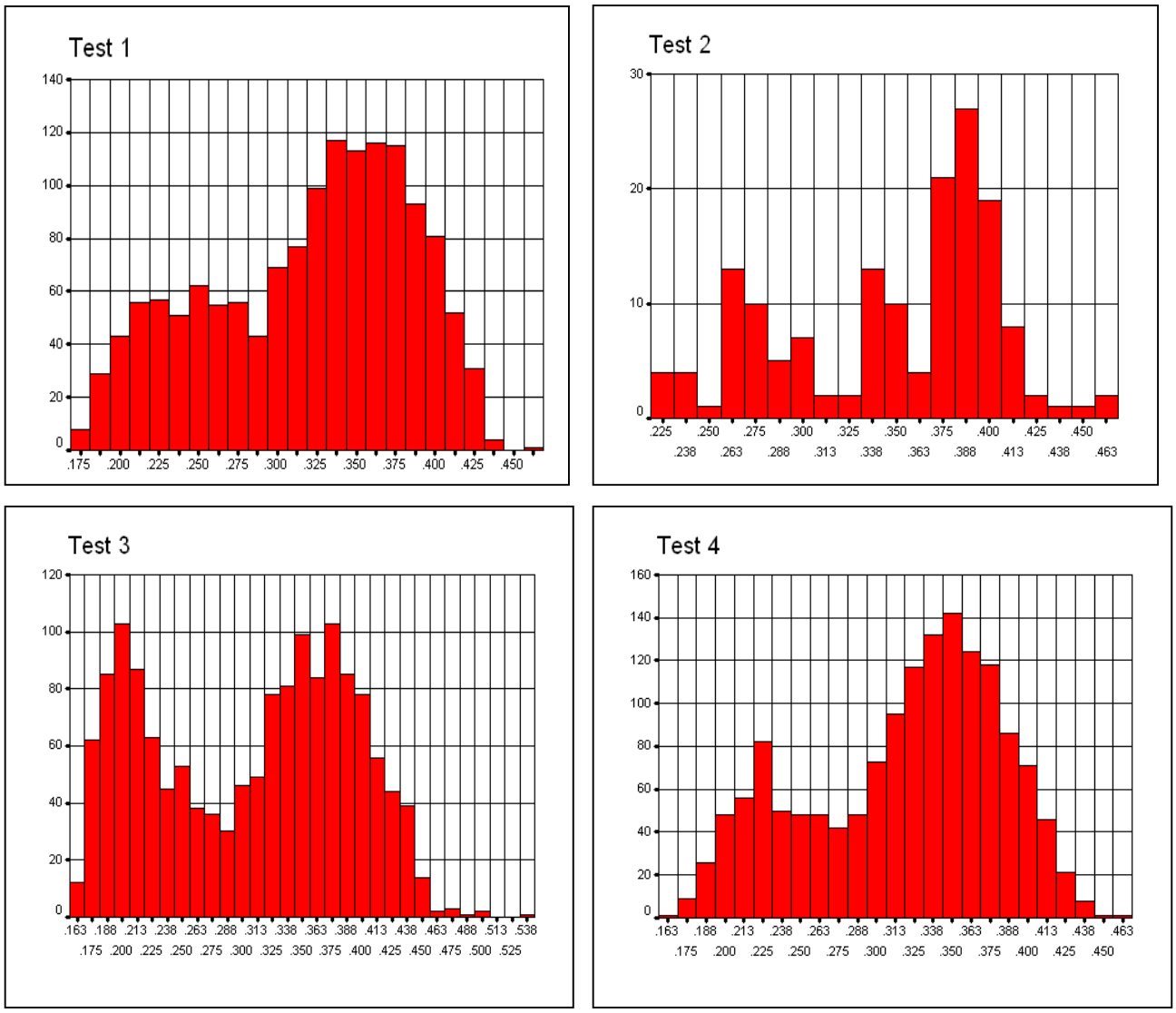

Figure 3 : FWHM Histograms

Figure 4 depicts the crystallite size mean rank results from the Kruscal-Wallis calculations and it indicates that Test 2 with fresh additives produces the smallest average crystallite size followed by Test 3 conducted with degraded additive, then Test 1 with no additive and finally Test 4 with an old additive as it would be expected. Figure 5 shows the median of crystallite size for all tests and confirms the above observation.

A comparison between the results in Tables 2 and 3 shows that while the surface roughness decreases in concert with a decrease in crystallite size between Tests 1 and 2; (as might be expected if crystallite size and particle size are closely related), the increases in surface roughness observed in Test 3 was not reflected in an increase in crystallite size. We are unable at this stage to explain this observation.

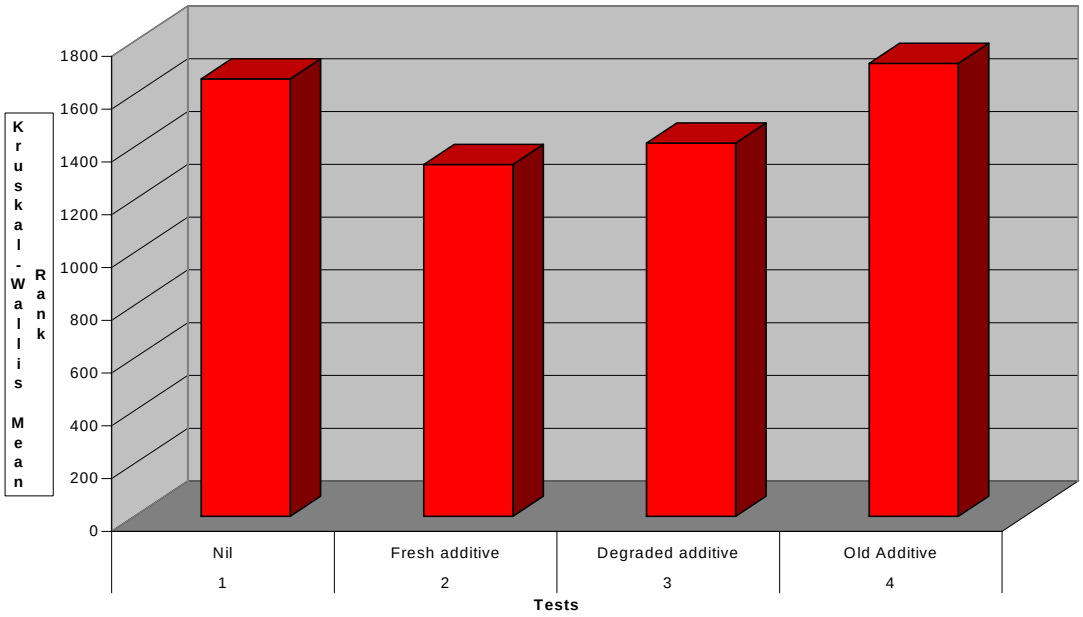

Figure 4: Kruskal-Wallis Mean Rank Results for Crystallite Size

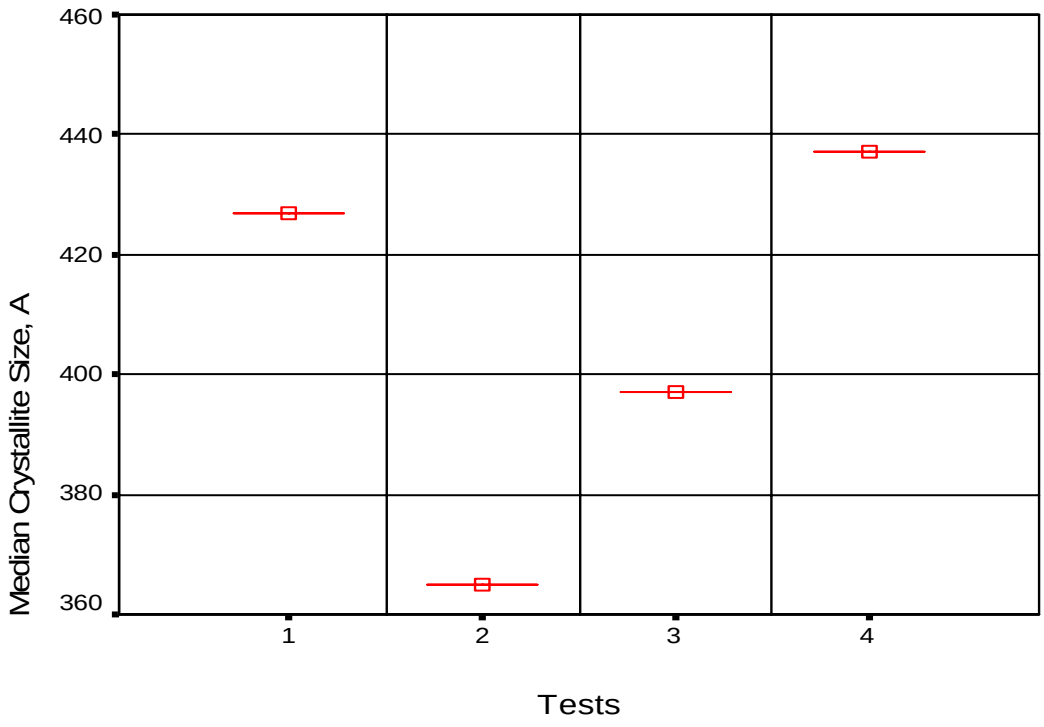

Figure 5: Median of Crystallite Size

Figure 6 shows the 3-D mapping of FWHM and crystallite size distribution for about 1450 readings per test for 2cm^2 surface area; except for Test 2 which had 150 readings on 1cm^2 area. It is noted that Test 3 indicates the predominance of smaller crystallite size. This figure demonstrates the ability of GADDS to obtain a map of crystallite sizes on electrowon deposits, a capability which potentially allows for a detailed study of spatially heterogeneous deposits.

Figure 8 shows a SEM micrograph of a polished sample of the electrowon copper in Test 3. It can be seen that a typical grain size as observed is of the order of 20μm. The median crystallite size for Test 3 measured by GADDS was 0.04μm indicating that for this sample an aggregation factor of the order of 500 is need to convert Scherrer crystallite size to the observable grain size.

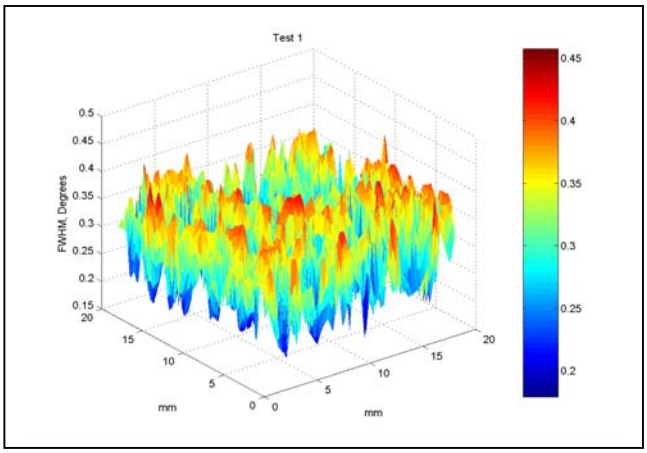
Test 1
FWHM, Degrees
mm
mm

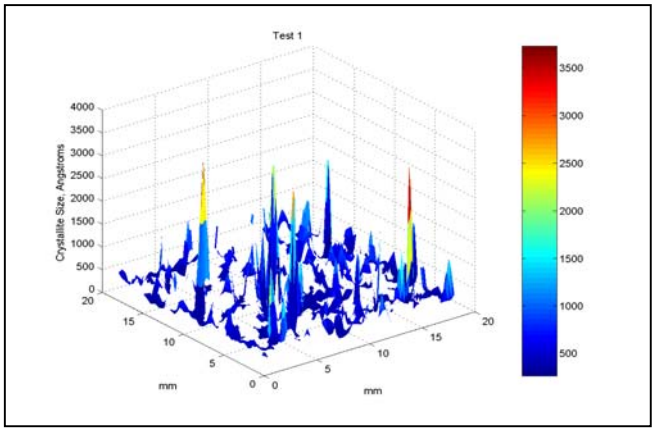
Test 1
Crystallite Size, Angstroms
mm
mm

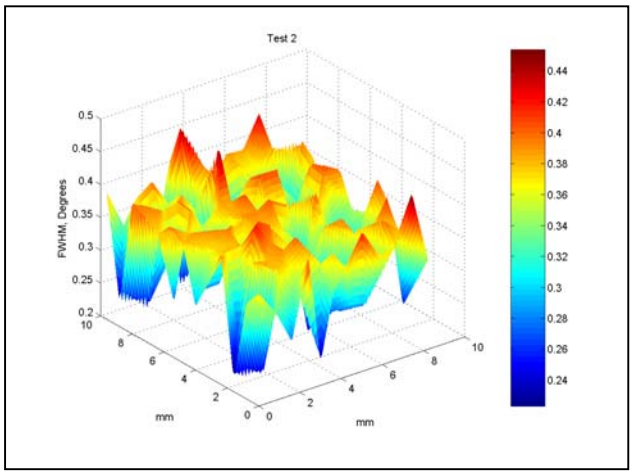
Test 2
FWHM, Degrees
mm
mm

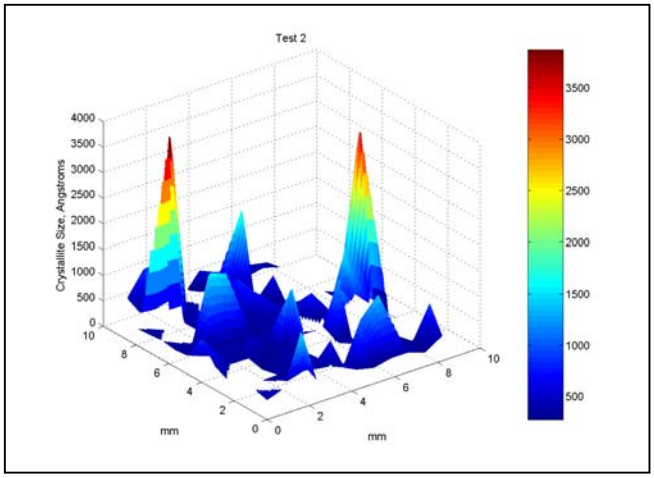
Test 2
Crystallite Size, Angstroms
mm
mm

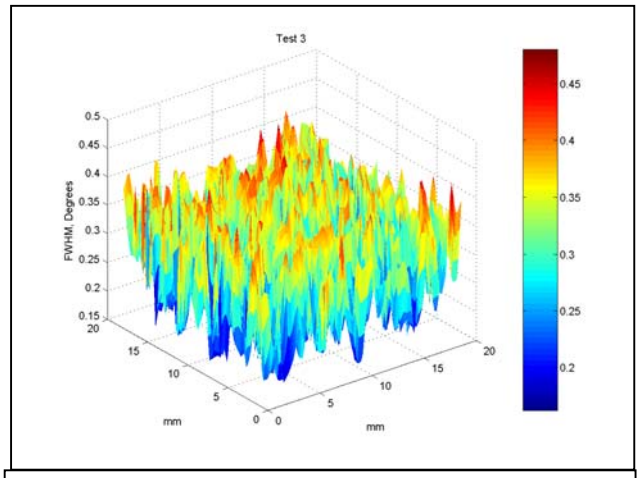
Test 3
FWHM, Degrees
mm
mm

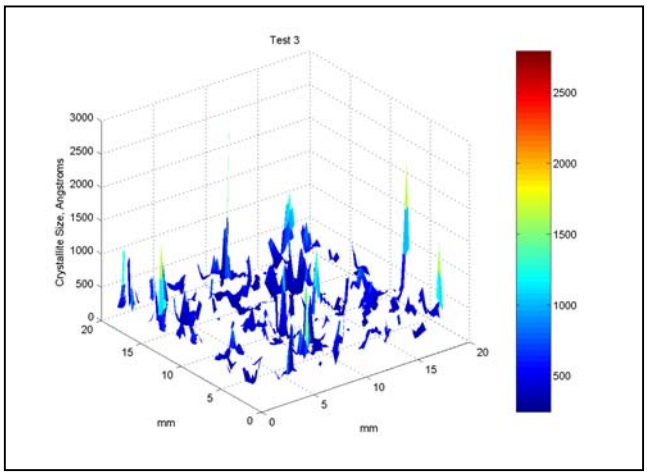
Test 3
Crystallite Size, Angstroms
mm
mm

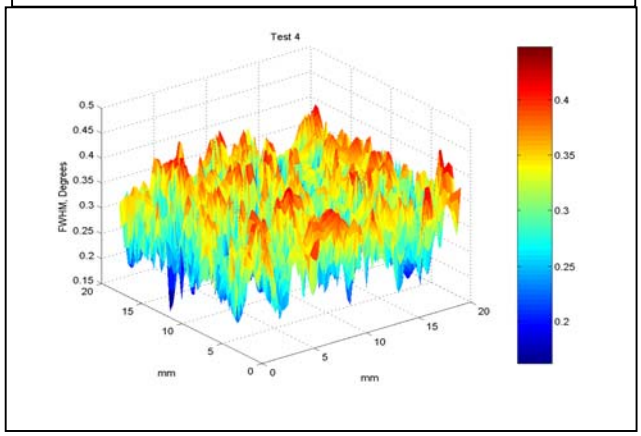
Test 4
FWHM, Degrees
mm
mm

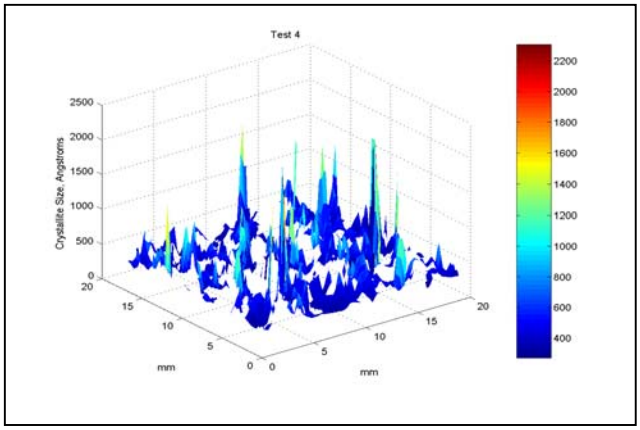
Test 4
Crystallite Size, Angstroms
mm
mm

Figure 6: 3D Mapping of FWHM and Crystallite Size

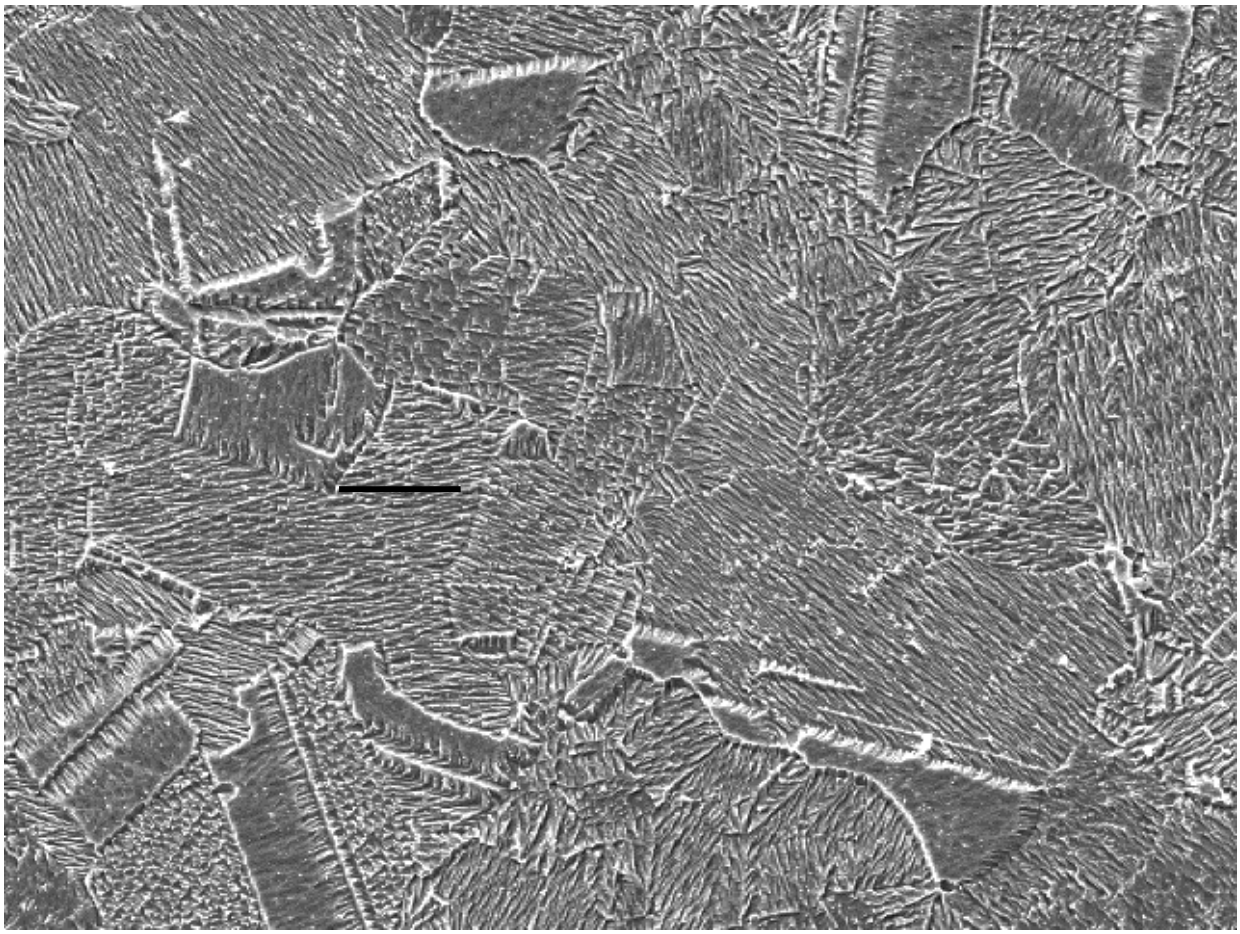

Figure 3: Test 3 Crystallite Size of Electrolyte-Side Polished (line = 20 μm)

Conclusions

In this paper we have demonstrated that GADDS, a non-destructive, in-situ technique is capable of detecting the effect of an additive on the crystallite size of electrowon copper. It was also shown that while there is some correlation between surface roughness and crystallite size, the correlation is relatively weak. In addition it has been demonstrated that GADDS allows for a study of spatial heterogeneity in crystallite dimension by allowing a 'map' of the crystallite size to be prepared.

Finally, additive "A" may be used as grain refiner in copper electrowinning and the GADDS technique may be used as a process control tool among other techniques, i.e., electrochemical, to select a new reagent system for copper electrodeposition in electrowinning, electrorefining and in the fabrication of interconnects.

Acknowledgements: we should like to acknowledge Mount Gordon Operations of Western Metals Copper Limited, Australia for supporting this research.

References

1. Budevski E, Staikov G, Lorenz W. Electrochemical Phase Formation and Growth, An Introduction to the Initial Stages of Metal Deposition. New York: VCH; 1996.
2. Moffat T, Bonevich J, Huber W, Stanishevsky A, Kelly D, Stafford G, et al. Superconformal electrodeposition of copper in 500-90 nm features. J. Electrochem. Soc. 2000;147(12):4524-4535.
3. Radisic A, West A, Searson P. Influence of Additives on Nucleation and Growth of Copper on n-Si(111) from Acidic Sulfate Solutions. Journal of the Electrochemical Society 2002;149(2):C94-C99.
4. Chassaing E. Effect of Organic Additives on the Electrocrystallization and the Magnetoresistance of Cu-Co Multilayers. Journal of the Electrochemical Society 2001;148(10):C690-C694.
5. Siemens, Bruker. GADDS Introduction Manual; 2001.
6. Klug H, Alexander L. X-Ray Diffraction Procedures for Polycrystalline and Amorphous Materials. Second ed. Sydney: John Willey & Sons; 1974.
7. MathSoft. Mathcad 2001i. In; 2002.
8. Price DC, Davenport WG. Densities, Electrical Conductivities and Viscosities of $CuSO_4/H_2SO_4$ Solutions in the Range of Modern Electrorefining and Electrowinning Electrolytes. Metallurgical & Materials Transactions B-Process Metallurgy & Materials Processing Science 1980;11B:159-163.
9. Price D, Davenport W. Physico-Chemical Properties of Copper Electrorefining and Electrowinning Electrolytes. Metallurgical & Materials Transactions B-Process Metallurgy & Materials Processing Science 1981;12B:639-643.
10. Baker DR, Verbrugge MW, Newman J. A transformation for the treatment of diffusion and migration. Application to the simulation of electrodeposition onto microelectrode geometries. Proceedings - Electrochemical Society 1992;92-3(Proc. Int. Symp. Electrochem. Microfabr., 1st, 1991):279-90.
11. Barkey D, Muller R, Tobias C. Roughness Development in Metal Electrodeposition I. Experimental Results. Journal of the Electrochemical Society 1989;138(8):2199-2207.
12. Uceda D. Determination of Mass Transfer Characteristics in the Electrolysis of Copper [PhD Thesis]. Missouri-Rolla: University Missouri-Rolla; 1988.
13. Ilgar E, O'Keefe T. Surface Roughening of Electrowon Copper in the Presence of Chloride Ions. In: Dreisinger D, editor. Aqueous Electrotechnologies: Progress in Theory and Practice; 1997: The Minerals Metals and Materials Society; 1997. p. 51-62.